

https://dspace.org/

# Comparing the performance of mobile and static LiDAR in detecting underground rock deformation

**Dlamini, Lubanzi Zolibonga Desree**

**2025**

University of the Witwatersrand, Johannesburg

https://hdl.handle.net/10539/50227

Dlamini, Lubanzi Zolibonga Desree. (2025). Comparing the performance of mobile and static LiDAR in detecting underground rock deformation. [Master's dissertation, University of the Witwatersrand, Johannesburg]. WIReDSpace. https://hdl.handle.net/10539/50227

Downloaded from a DSpace repository. https://dspace.org/




# Comparing the performance of mobile and static LiDAR in detecting underground rock deformation

MSc Research Thesis

Lubanzi Zolibonga Desree Dlamini (1345070)

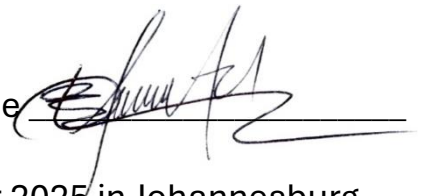
**Supervisor**
Prof Elhadi Adam

**Co-Supervisors**
Dr Iqra Atif

Submitted in fulfilment of the requirements for the degree of Master of Science in Geography in the School of Geography, Archaeology and Environmental Studies, Faculty of Science, University of the Witwatersrand
2025

## Declaration

I, Lubanzi Zolibonga Desree Dlamini, hereby declare that this research report is my original work. I am submitting it for the Degree of Master of Science in Geography at the University of the Witwatersrand, Johannesburg. This report has not been submitted for any other degree or examination at any university.

Signature of Candidate 

12th day of September 2025 in Johannesburg

# Abstract

Accurate deformation monitoring is essential for ensuring structural stability in underground mining environments. This study, therefore, evaluates the performance of mobile and static LiDAR scanners in capturing and analysing rock deformation within a controlled underground mock mine. The point cloud data was collected pre- and post-deformation using both scanning platforms and was processed in the open-source CloudCompare for registration, segmentation and deformation analysis. The comparative assessment focused mainly on point cloud characteristics, surface errors and deformation mapping accuracy. The comparative results show that static LiDAR has a higher point resolution and lower surface errors, while mobile LiDAR allows for rapid data acquisition with a broader spatial coverage. Deformation measurements obtained from both platforms show a strong correlation with the field measurements; this is confirmed by statistical analysis with $R^2$ Values greater than 0.99. Furthermore, a paired t-test resulting in a p-value of 0.188 exceeded the commonly used threshold of 0.05, indicating no significant difference between the two methods. Moreover, a trade-off between accuracy and operational efficiency was identified; where static LiDAR ensures high data quality, it is constrained by occlusions and acquisition time. Meanwhile, mobile LiDAR is more adaptable to confined environments. These findings contribute to optimising LiDAR-based deformation monitoring strategies in underground mining, balancing precision, efficiency, and practical implementation.

## Acknowledgements

I gratefully acknowledge the Mine Health and Safety Council (MHSC), South Africa and Sibanye-Stillwater Digital Mining Laboratory (DigiMine) for sponsoring this research. My sincere thanks to Dr. M. Ahsan Mahboob (Head of DigiMine) for his support. I also extend my appreciation to Mr. Barrend Bornman (Leica Geosystems) for providing scanning equipment and assisting with data acquisition.

I am deeply indebted to my supervisors, Prof. Elhadi Adam, for his unwavering guidance, and Dr. Iqra Atif, for her expertise. Their mentorship was pivotal to this project's success.

To my husband, family, and friends, thank you for your endless encouragement and prayers. Finally, I dedicate this work to my two beloved children, Wazumusa and Mihle, whose arrivals during the course of this research made this journey unforgettable.

# Contents

**Declaration** ..... **i**

**Abstract** ..... **ii**

**Acknowledgements** ..... **iii**

**List of Tables** ..... **xi**

**Chapter 1** ..... **1**

**1 Introduction** ..... **1**

1.1 Background of the study ..... 1

1.2 The prevalence of rock deformation in underground mining ..... 3

1.3 Problem Statement ..... 4

1.4 Amis and Objectives ..... 5

1.4.1 Research Hypotheses ..... 5

1.5 Scope of the thesis ..... 5

**Chapter 2** ..... **8**

**2 Literature Review** ..... **8**

2.1 Introduction ..... 8

2.2 Deformation monitoring in underground mines ..... 8

2.3 Horizontal and vertical deformation ..... 9

2.4 Causes of ground deformation in underground mining ..... 10

2.5 Underground rock deformation structures ..... 12

2.6 Risk and Hazards in Underground Mines ..... 15

2.7 Importance of underground Deformation monitoring ..... 16

2.8 Monitoring underground deformation using different technologies ..... 17

2.8.1 Ground-Based Monitoring Instruments ..... 17

2.8.2 Remote Sensing-Based Deformation Monitoring Methods ..... 19

2.8.3 Wireless Sensor Networks (WSNs) ..... 20

2.8.4 Fiber Optic Sensors ..... 20

2.8.5 Radar-Based Monitoring ..... 21
2.8.6 Internet of Things (IoT) ..... 22
2.8.7 Optical Methods ..... 22
2.8.8 Light Detection and Ranging (LiDAR) ..... 23
2.9 Working principles of LiDAR remote sensing ..... 28
2.9.1 LiDAR platforms and their working principle ..... 30
2.9.2 Terrestrial Laser Scanning ..... 31
2.9.3 Terrestrial mobile laser scanning ..... 31
2.10 Georeferencing methods for terrestrial LiDAR Scanning ..... 32
2.10.1 Conventional Georeferencing Approach ..... 32
2.11 Point cloud data management ..... 32
2.12 Identified knowledge gap. ..... 33
**Chapter 3 ..... 35**
**3 Methods and Materials ..... 35**
3.1 Introduction ..... 35
3.2 Research Design and Approach ..... 35
3.2.1 Displacement Measurement Process: Pre- and post-deformation ..... 35
3.3 Study site ..... 39
3.4 Environmental Controls ..... 40
3.5 Instrumentation ..... 41
3.5.1 LiDAR Scanners ..... 41
3.5.2 Control Survey Equipment ..... 43
3.6 Data processing ..... 44
3.7 Data Collection ..... 46
3.7.1 Identifying and Mapping Rock Deformation (Objective A) ..... 46
3.8 Maximum distance computation as displacement ..... 47

3.9 Evaluating the Accuracy of Static and Mobile LiDAR (Objective B) ..... 48
3.9.1 Total Station Georeferencing: ..... 48
3.9.2 LiDAR Point Cloud Registration: ..... 50
3.10 Metrics for accuracy and reliability assessment: ..... 52
3.10.1 Root Mean Square Error (RMSE) ..... 52
3.10.2 Mean Absolute Error (MAE) ..... 53
3.10.3 Coefficient of Determination ($R^2$) ..... 53
3.10.4 Paired t-Test ..... 53
M3C2 Algorithm for Deformation Analysis ..... 54
**Chapter 4 ..... 56**
**4 Results ..... 56**
4.1 Introduction ..... 56
4.2 Post-Processing Comparison of Static and Mobile LiDAR ..... 56
4.2.1 Point Cloud Characteristics ..... 57
4.2.2 Point cloud registration ..... 58
4.3 Deformation Mapping and Visualisation ..... 60
4.4 Deformation Measurement Accuracy ..... 65
4.4.1 Statistical Analysis ..... 66
4.5 Assessing the operational efficiency of static and mobile LiDAR systems in detecting rock deformation. ..... 69
4.6 Discussion ..... 71
4.6.1 Identifying and Mapping Rock Deformation in the Underground Mining Environment ..... 71
4.6.2 Comparative Analysis of Deformation Measurement Accuracy ..... 71
4.6.3 Operational Efficiency and Trade-offs of Static and Mobile LiDAR Systems 72
4.6.4 Assessment of Data Quality Limitations ..... 72

4.7 Limitations and Systematic Biases ..... 72
4.8 Cost-Efficiency Analysis ..... 73
**Chapter 5 ..... 74**
**5 Conclusion and Recommendations ..... 74**
5.1 Introduction ..... 74
5.2 Actionable Recommendations ..... 74
5.3 Conclusion ..... 75
6 References ..... 76

# List of Figures

Figure 1: A 20-year record (2003-2023) classification of underground mining fatalities, showing ground falls as one of the leading causes of fatalities (MHSC, 2024). ..... 2
Figure 2: Factors such as in-situ stress, rock mass quality, rock brittleness, support effectiveness, siesmicity, local mine stiffness, geological structures, opening size and orientation, and excavation sequence may cause rock deformation. (Cai, 2024). ..... 10
Figure 3: Summarization of the occurrence and characteristics boulder weathered rock mass (M. Dan *et al.*, 2016) ..... 13
Figure 4: Isolated semi-circular rock mass in a mine roof. With a rounded or flat bottom when viewed from below (Kentucky Geological Survey, (2019)) ..... 14
Figure 5: Observed damage to the brattice wall, shaft concrete lining and the sidewall of the 64 Level station (Judeel, 2003). ..... 14
Figure 6: Development of rockbursts on rock surface: (a) Surface of an opening, (b) growing cracks, (c) A slab, and (d) Buckling (Deng et al., 2019). ..... 15
Figure 7: The framework of ground control with IoT in underground coal mines (Hao et al., 2020) ..... 22
Figure 8: Acquisition process for deformation simulation and measurement. ..... 36
Figure 9: Technical process for calculating deformation based on point cloud data. ... 38
Figure 10: Chamber of Mines building. (a) The mock “underground mine” tunnel at the lower ground section of the building. (b) A weather station situated on the roof of the main building signifies the surface of the mock underground mine. ..... 39
Figure 11: Image of the tunnel displaying rock formations, artificial lighting, ventilation pipe and blasting system. ..... 40
Figure 12: The static tripod mounted terrestrial laser scanner used was the RTC 360 .. 41
Figure 13: Leica BLK2GO Handheld Imaging Laser Scanner (Leica Geosystems, 2022). ..... 43
Figure 14: Total station and target set up to determine the coordinates and height of the three tie points. ..... 44
Figure 15: Irregular boulder structure randomly placed as an unstable cornerstone at the face of the tunnel to simulate the concept described by Dan et al., (2016). ..... 46

Figure 16: Deformation simulation of a semi-circular rock mass, sagging from an underground mine roof ..... 47
Figure 17: Underground tunnel displaying pre-and post-deformation simulation for rock burst scenario on the tunnel's rock surface ..... 48
Figure 18: Target network of three tie points (ST1, ST2, ST3) selected for the registration of the laser data ..... 49
Figure 19: Registration of scans to a unified coordinate system, showing a closed-loop trajectory of mobile laser scanning with total station positions and computed X, Y, and Z values. ..... 51
Figure 20: Static and mobile LiDAR point cloud model of the tunnel, with the red block showing the segmented section along the tunnel where the analysis occurred. ..... 56
Figure 21: Post-processing contrast of segmented, pre- and-post deformation point-cloud scans from both static and mobile LiDAR platforms ..... 57
Figure 22: Comparison of occlusion effects in static and mobile LiDAR scans. A (static LiDAR), occlusion is visible behind the object leaving gaps due to restricted line of sight. B (mobile LiDAR), reduced occlusion because of moving scanner capturing multiple perspectives ..... 58
Figure 23: Reconstructed 3D surface models for pre- and post-deformation segments of the tunnel. ..... 60
Figure 24: Computation of maximum/minimum deformation distance from detected areas of deformation using statistical computation function. Deformation areas are colour-coded, with warm colours indicating outward deformation and cool colours showing inward deformation. ..... 62
Figure 25: Contrast of static and mobile LiDAR segments, presenting localised deformations. Warm colours (red and yellow) indicate outward deformation or material addition, and cool colours (blue and green) signify inward deformation or material loss. ..... 63
Figure 26: Contrast of static and mobile LiDAR face segments, presenting localised deformation. ..... 64
Figure 27: Comparison of deformation measurements computed from the LiDARs tested against the ground truth measurements. ..... 66

Figure 28: $R2$ relationship between deformation measurements obtained from a) mobile LiDAR, b) static LiDAR and ground truth data field measurements ..... 68

# List of Tables

Table 1: Traditional rock deformation monitoring methods used in underground mining 2
Table 2: Comparison of underground rock deformation monitoring methods, their applications, advantages and disadvantages. ..... 25
Table 3: Software used to capture and process the raw point data. ..... 45
Table 4: Surface errors for the different segments of the tunnel. Surface errors were generated after fine-registering the pre- and post-deformation scans with one another. ..... 58
Table 5: Comparison of deformation measurements for the simulated formations was measured using field methods and static and mobile LiDAR platform measurements. 65
Table 6: RMSE for mobile and static LiDAR calculated from ground field measurements vs LiDAR data. ..... 67
Table 7: MAE for mobile and static LiDAR calculated from ground field measurements vs LiDAR data. ..... 67
Table 8: Overview of operational efficiency of static and mobile lidar systems. ..... 69

# Chapter 1

## 1 Introduction

### 1.1 Background of the study

Rock deformation in mining areas is the gradual change in the shape, size and volume of the rock formation because of natural and mining-induced factors (Molinda & Mark, 2010). These changes can significantly compromise structural stability and integrity, ultimately posing safety hazards and operational efficiency. Rock deformation or the unplanned falls of ground incidents may be caused by mining activities such as blasting and excavation, which alter the stress distribution of the enclosing rock (Xia *et al.*, 2016). It may also result from natural stresses within the Earth's crust caused by the dynamic movement of rocks and environmental factors such as changes in temperature, water infiltration, and seismic events. These deformations serve as early warnings that precede catastrophic rock failures (Wang & Zheng, *et al.*, 2017).

In South Africa, the mining industry has been the backbone of the country's economy (Cowling, 2023), and over the decades, continuous extraction of precious resources has led to deep-level mines. The Witwatersrand Basin, particularly, hosts some of the world's deepest mines, where rock deformation incidents (Figure 1) have been a constant challenge (Riemer & Durrheim, 2012). This is why the Mining Health and Safety Council (MHSC) has prioritised addressing the issue of falls of ground through its "Net-Zero-Harm" and "Fall of Ground Action Plan (FOGAP)" campaign that aims to achieve a mining industry that operates with zero harm to its workforce. This has been addressed by enhancing monitoring technologies, like ground penetrating radar, seismic monitoring, and light detection and ranging (LiDAR) monitoring systems to detect and assess rock deformation in real time. Currently, the health and safety statistics of South Africa's underground mining industry identify falls of ground as one of the leading causes of casualties (MHSC, 2023), and internationally, regions like Australia, Canada, and the United States also face similar problems, especially in large-scale underground mining operations (CDC, 2024; East, 2025).

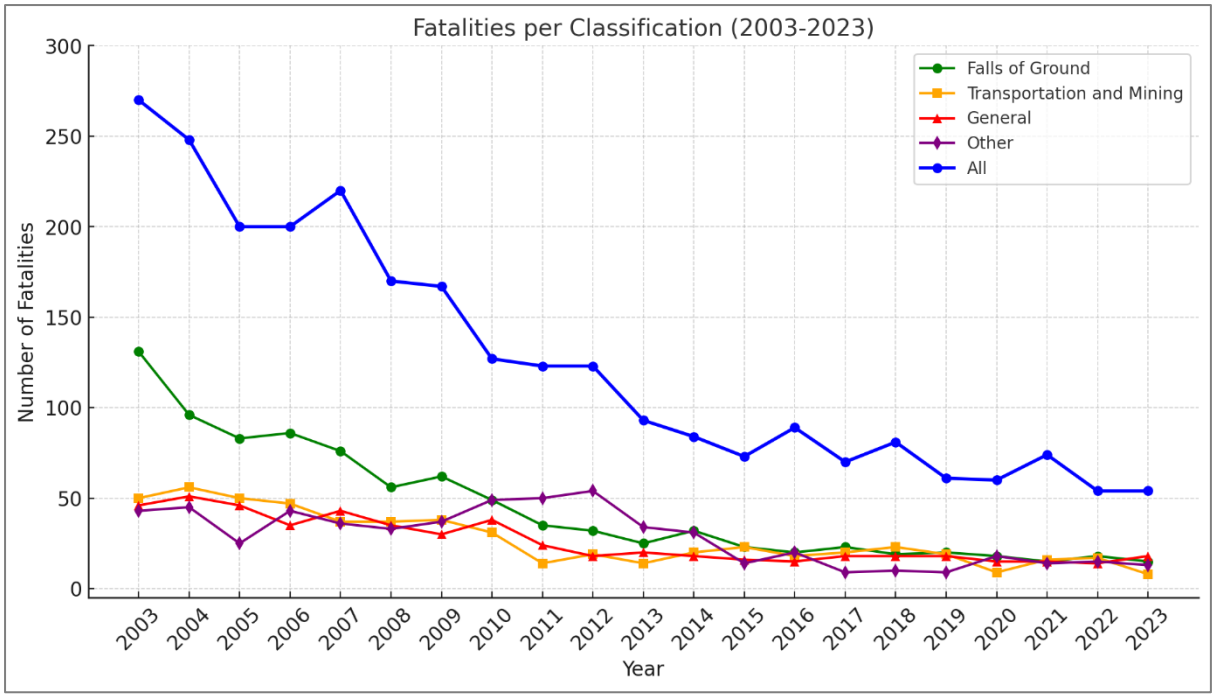



Figure 1: A 20-year record (2003-2023) classification of underground mining fatalities, showing ground falls as one of the leading causes of fatalities (MHSC, 2024).

Understanding and monitoring rock deformations is vital for maintaining safe working spaces, properly planning designs, and choosing the correct mining method for improved safety and efficient operation (Zeng *et al.*, 2020). The conventionally used manual and basic traditional monitoring methods have been used to create a safe environment for the mining (Table 1). However, the methods are time-consuming and labour-intensive, with limited spatial coverage (Delaloye, 2012; Yang *et al.*, 2017a).

Table 1: Traditional rock deformation monitoring methods used in underground mining

| **Manual methods** | **Working principle** | **Limitations** |
|---|---|---|
| Visual inspection, audio assessment (Green & Mikkelsen, 1988) | Miners visually inspect spaces for signs of cracks, bulges and rock displacement. Hitting rock with a rod releases sounds that distinguish between solid (clear, ringing sound) and fractured (dull, hollow sound) rocks. | No quantitative data, inaccurate and presumptuous, labour intensive, time-consuming, high-risk, limited coverage |

| **Basic instrument methods** | | |
|---|---|---|
| Tape measures, inclinometers (Slaker & Mohamed, 2017) | Assess changes in rockface angles, displacement, structural integrity | Limited spatial coverage, permanent installation, periodic measurement, risk of damage, prone to environmental factors, high maintenance, costly |
| Extensometers, load cells (Cota & de Figueiredo, 2014) | Mounted on surfaces to monitor stress and loads. Monitor strain and small changes in rock movement. | |

### 1.2 The prevalence of rock deformation in underground mining

The catastrophic repercussions of this phenomenon manifest as subsidence, ground movement and rock bursts. The manifestation of deformation varies due to differences in geological formations, mining techniques and regulatory frameworks.

In South Africa, the geological conditions are challenging and characterised by high-stress environments due to the deep mining operations, complex rock structures and seismic activity. This, therefore, leads to frequent rock deformation events (Brink *et al.*, 2008). In 2019, the Department of Mineral Resources and Energy (DMRE) reported 369 accidents, 385 injuries, and 20 deaths (DMRE, 2021). In North America, in regions like Canada and the United States, underground mining operations occur in varied geological settings, from hard rock mines to coal mines. Rock deformation issues include subsidence, especially in the coal mining regions, and seismicity in hard rock mines. Over 20 mines in Canada have encountered rock burst accidents. In the United States, between 1936 and 1993, a total of 172 recorded rockburst events resulted in 78 fatalities and 158 injuries (Mark, 2016; Pu *et al.*, 2019). Australia's mining sector also famous for its extensive mining industry, experiences challenges with the rock deformation phenomenon, although renowned to be one of the safest in the world. A 2023 North South Wales Government Safety bulletin reported a rise in rockfall injuries to workers in underground mines (NSWG, 2023). Seismic events and ground movement are prevalent, and their geology requires complex structures that require robust monitoring and support systems (Rahimi *et al.*, 2020). European underground mines, such as those in

Poland, Britain and Germany, deal with deformation issues related to coal mining and other mineral extractions. Subsidence and water ingress are common problems exacerbated by the shallow depth of many operations and historical mining activities (Strzałkowski, 2021). Asian Countries, such as China and India, have a high density of coal mining activities and varying geological conditions, contributing to frequent deformation incidents (Chen, 2020). Rock bursts in these underground coal mines normally occur in mining roadways due to disruption of the equilibrium of the surrounding rock and coal system. For 2510 recorded rock burst data points, 2178 events occurred in mining roadways, accounting for 86.8% of the recorded total (Chen *et al.*, 2023).

### 1.3 Problem Statement

Underground mining environments are inherently unstable due to unpredictable geological conditions and constant rock mass movements. These movements are induced by drilling, blasting, and other mining processes (Deng *et al.*, 2019). Catastrophic failures occur if these rock deformations are left undetected or insufficiently monitored. Falls of ground (FOG) are identified by the Mining Health and Safety Council (2023) as the leading cause of casualties and fatalities in underground mining and pose significant human health and safety hazards. Additionally, FOG incidents delay operations, resulting in substantial financial losses for mining companies (Molinda & Mark, 2010). Existing deformation monitoring methods, including traditional visual inspections and ground-based instruments, often lack the spatial coverage and precision necessary for effective risk assessment. This situation highlights the need for advanced real-time and high-resolution monitoring technologies.

LiDAR (Light Detection and Ranging) remote sensing technology emerges as a powerful tool for capturing three-dimensional mapping of underground mining environments (Pinpin *et al.*, 2021; Singh *et al.*, 2021). However, choosing between static LiDAR and mobile LiDAR presents a critical challenge in underground deformation monitoring. While static LiDAR scanners offer high accuracy and dense point cloud data, they are time-intensive, and their fixed position limits their coverage (Trzeciak & Brilakis, 2021). On the contrary, mobile LiDAR provides rapid data acquisition and improved

accessibility in confined spaces but may introduce motion-induced errors and lower spatial resolution (Lindenbergh & Pietrzyk, 2015a). The trade-offs between accuracy, efficiency and operational feasibility require evaluation to determine the most effective approach for underground mining applications.

Despite LiDAR's increased adoption in deformation monitoring, research comparing static and mobile LiDAR in underground mines remains limited. Addressing this gap, the study intends to assess and compare the accuracy, surface errors, and operational efficiency of these technologies. The findings will help optimise deformation monitoring strategies, enhancing safety and decision-making in underground mining environments.

## 1.4 Amis and Objectives

This study aims to compare the efficiency of mobile and static LiDAR in detecting rock deformation of underground mines in the GIS environment.

Specific objectives

The main research objectives are to:

a) Identify and map rock deformation in the underground mining environment.
b) Evaluate the accuracy of static and mobile lidar for deformation monitoring
c) Examine the operational efficiency of static and mobile lidar systems.

### 1.4.1 Research Hypotheses

Hypothesis ($H_1$):

Mobile and static LiDAR systems significantly differ in their accuracy for detecting and mapping rock deformation in underground mining environments.

Null Hypothesis ($H_0$):

There is no significant difference between mobile and static LiDAR systems in terms of accuracy for detecting and mapping rock deformation in underground mining environments.

## 1.5 Scope of the thesis

The thesis is structured into five chapters, each systematically addressing various components of the study. Chapter 1 introduces the research problem and its significance, while Chapter 2 provides a comprehensive literature review on

underground deformation and monitoring technologies. Chapter 3 covers the experimental methodology, including data collection and analysis techniques. The results are presented and discussed in Chapter 4. With a summary of results, recommendations, and future research directions, Chapter 5 closes the study.

**Chapter 1**

This introductory chapter overviews the critical issue of rock deformation in underground mining environments, highlighting its importance and implications for safety and operational efficiency. It gives the importance of monitoring deformation, focusing on South Africa's deep-level mining, which has significant challenges. It briefly introduces traditional methods and their limitations, prompting the exploration of advanced technologies like static and mobile LiDAR.

**Chapter 2**

Chapter 2 is the literature review, and it delves into underground mining rock deformation and the technologies used to monitor it, highlighting their importance for safety and operational efficiency**.** The chapter discusses how various mining methods affect ground stability and explains why monitoring ground deformation is essential. The chapter compares various deformation monitoring technologies: Ground-Based Instruments, Remote Sensing Methods, Advanced Techniques, and Optical and LiDAR Technologies. Chapter 2 underscores the significance of choosing appropriate monitoring technologies to ensure safety, stability, and efficiency in underground mining operations.

**Chapter 3**

Chapter 3 outlines the methodology for experimental deformation monitoring in an underground mock mine using Mobile and Static LiDAR scanners. Both Mobile and Static LiDAR scanners capture point clouds at different epochs. The underground mock mine provides a controlled environment to simulate real mining conditions. The collected point clouds are analysed using the CloudCompare software. Statistical comparisons between field measurements and LiDAR-derived data are conducted to evaluate the accuracy and reliability of the two platforms.

**Chapter 4**

This results chapter presents the findings and discusses the analysis of the deformation monitoring. The deformation patterns are visualised, highlighting the significant changes identified along the tunnel. The analysis includes generating 3D models, detecting and visualising deformations, and quantifying changes between scans. The results are used to evaluate each scanning method's effectiveness in identifying potential areas of instability or deformation. Discrepancies arising from data gaps and meshing limitations are discussed. The integration of visual, quantitative and qualitative analyses aims to demonstrate the effectiveness of LiDAR-based deformation monitoring.

**Chapter 5**

The conclusion chapter provides a comprehensive summary of key findings. Recommendations are proposed to address observed data quality challenges, including strategies for minimising data gaps and optimising point cloud acquisition and processing techniques. Finally, suggestions for future research are provided, focusing on improving LiDAR methodologies and applications in diverse underground settings to enhance the robustness and accuracy of deformation monitoring practices.

# Chapter 2

## 2 Literature Review

### 2.1 Introduction

This chapter unpacks deformation monitoring as a critical component of ensuring safety and stability in underground mining environments, where ground movements pose significant risks to infrastructure, equipment, and personnel. It reviews the key aspects of deformation monitoring, beginning with its role in underground mines and distinguishing between horizontal and vertical deformation. Then, it explores the causes of ground deformation and associated risks and hazards, emphasising the necessity of effective monitoring. Various technologies for underground deformation monitoring are discussed, including a comparison of their applications, advantages, and limitations. The principles and techniques of LiDAR remote sensing are introduced, followed by georeferencing methods for terrestrial LiDAR scanning. Finally, point cloud data management is addressed, highlighting its significance in data processing and analysis.

### 2.2 Deformation monitoring in underground mines

Deformation monitoring of underground mines is an engineering practice that aligns closely with the regulatory framework stipulated in South African mining legislation. South Africa has a rich mining history, and the mining industry contributes significantly to the country's economy. (Cowling, 2023). Over the years, the Mines Health and Safety Act 29 of 1996 was established as the principal legislative framework governing health and safety standards in mining operations. This piece of legislation emphasises inclusive risk assessments and monitoring mechanisms, making rock monitoring an imperative component of ensuring compliance with safety standards (MHSC, 2023). The diverse geological nature of South Africa's mining environment is characterised by various rock types and formations, which necessitate tailored deformation monitoring strategies unique to each formation. The National Environmental Management Act (NEMA) and the Mineral and Petroleum Resources Development Act (MPRDA) further contribute to the regulatory framework, emphasising the need for sustainable mining practices and environmental responsibility.

In practical terms, deformation monitoring in underground mines is mainly used to detect abnormal shifts or changes in the enclosing rock mass; this is essential for ensuring the safety of mine workers and preventing rockfall accidents (Singh *et al.*, 2023). Real-time monitoring can alert mining operators to potential hazards, such as ground instability or rockfalls, allowing for timely evacuation and intervention (Brink *et al.*, 2008). Underground mines are supported by a network of tunnels, shafts, and other structures (Rahimi *et al.*, 2020), monitoring deformation helps assess the structural integrity of these components by identifying deformations or movements so that mining engineers can take corrective measures to reinforce structures, preventing collapses and ensure the long-term stability of the mine (Monika *et al.*, 2023).

There are two types of strain or movement that occur within the rock formations surrounding underground mine workings: vertical and horizontal rock deformation (Xia *et al.*, 2016). These deformations need to be closely monitored as they can have significant implications for mine safety, stability, and productivity. Efficient mining operations rely on stable and predictable conditions, and deformation monitoring provides valuable information that can be used to enhance resource allocation (Jacobs, 2016). For example, if an area of the mine is experiencing excessive deformation, mining activities can be modified to minimise risks and maximise ore extraction.

### 2.3 Horizontal and vertical deformation

Monitoring rock deformation in underground mines is essential to maintaining the stability and safety of the working environment. Both vertical and horizontal deformation are important indicators of potential hazards such as rock bursts, collapses, or roof falls (Agapito & Gilbride, 2002; Shukun Zhang *et al.*, 2021). Whereas horizontal deformation is concerned with lateral movements or shifts in the rock strata, vertical deformation is defined as changes in the height or elevation of the rock mass (Zhao *et al.*, 2023).

Instruments such as extensometers, borehole cameras, or laser scanning systems are used to detect vertical deformation (Kavvadas, 2003; Cota & de Figueiredo, 2014). These can track changes in distance between reference points or the movement of rock strata over time. Similarly, horizontal deformation monitoring involves using inclinometers, strain gauges, or tiltmeters to track shifts in the horizontal plane (Green & Mikkelsen,

1988; NSW Government Agency, 2021). Identifying variations in angles or alignments within the rock structure offers important insights into possible structural weaknesses or stress concentrations (Małkowski *et al.*, 2020).

Integrating information from horizontal and vertical deformation monitoring systems provides a thorough grasp of the dynamic behaviour of subterranean rock masses (Seymour *et al.*, 2019; Xia *et al.*, 2022). Proactive risk management is made possible by this integrated strategy, improving safety standards and reducing the possibility of mishaps or disturbances in mining operations (Wang *et al.*, 2023). Ultimately, maintaining production and protecting workers' safety depends heavily on effectively monitoring rock deformation.

## 2.4 Causes of ground deformation in underground mining

Ground deformation in underground mining is a complex phenomenon influenced by countless factors related to natural geological conditions and human activities associated with mining, as shown in Figure 2.

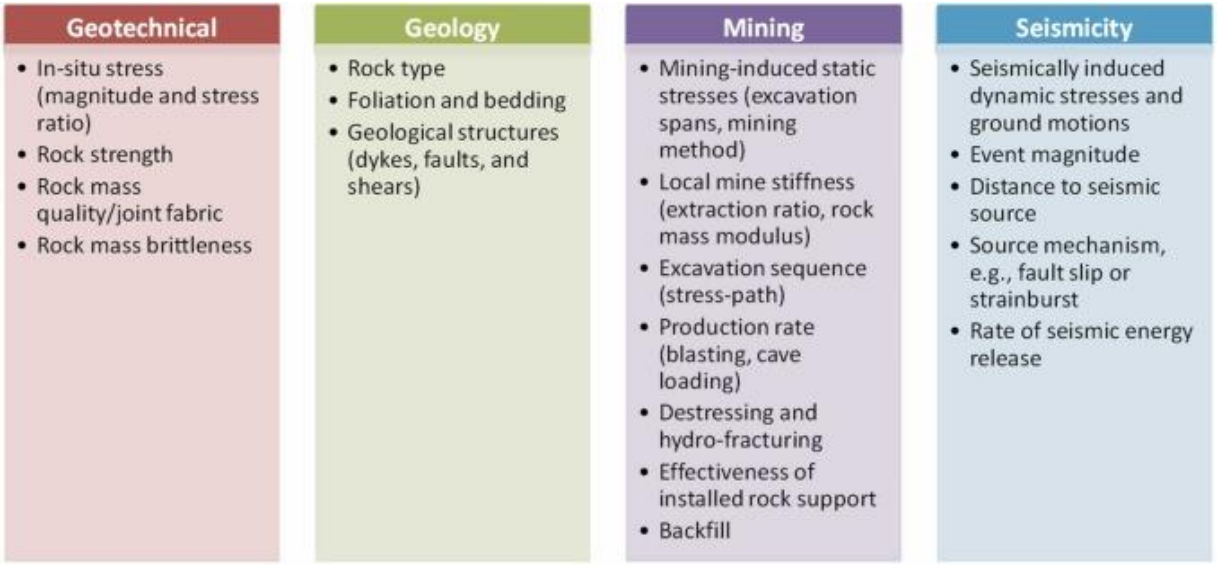



Figure 2: Factors such as in-situ stress, rock mass quality, rock brittleness, support effectiveness, siesmicity, local mine stiffness, geological structures, opening size and orientation, and excavation sequence may cause rock deformation. (Cai, 2024).

The following are some key factors that may contribute to ground deformation:

*a) Extraction of Minerals*

The primary cause of ground deformation in underground mining is the extraction of minerals from the earth. As mining activities progress, voids are created in the rocks from

which ore is removed (Baghbadorani *et al.*, 2021). These voids can lead to subsidence, causing the ground above to settle. The extent of subsidence depends on factors such as the mining method, ore body geometry, and the mechanical properties of the surrounding rock (Jianjun *et al.*, 2021; Wang *et al.*, 2021).

*b) Rock Stress Redistribution*

Mining operations can alter the natural stress distribution within the rock mass. In an experimental study of five underground coal mines, Zeng *et al.*, (2020) alludes that due to ore extraction, the stress on the remaining rock changes, leading to the adjustment of the surrounding rock. This redistribution of stress can result in ground movements, including horizontal and vertical deformations. They further conclude that understanding and managing these stress changes is crucial for maintaining the stability of the underground environment. In some mining regions, seismic activity may contribute to ground deformation. Earthquakes or mining-induced seismic events can cause sudden shifts in the subsurface, affecting the stability of underground structures (Wu, 2021). Jennifer and Porchelvan (2021) Elaborate on seismic activities, reviewing case studies from South Africa, Korea, and Sweden. Citing the importance of monitoring and understanding the seismic risk in a mining area for proactive risk management even post closure.

*c) Geological Conditions*

The geological characteristics of the rock and soil surrounding a mining operation play a significant role in ground deformation. Different rock types have varying mechanical properties, and the presence of faults or fractures can influence the stability of the ground. Khan *et al.*, (2022), attest to this in their study of 5 different mines in China, where they analysed correlations between microseismic events and varying regional stratigraphy during various seismic events. Geological mapping and continuous monitoring help identify potential risk areas prone to deformation based on the specific geological conditions (Singh *et al.*, 2023).

*d) Mining Methodology*

The choice of mining method has a direct impact on ground deformation, and over the years, mining technology and methods have progressively improved to reduce

catastrophes (He *et al.*, 2021). In an investigation, Li *et al.*, (2022) explores stratum and surface deformation in an underground phosphorite mine using different mining methods. Exploring methods such as room and pillar, longwall mining, or block caving, each method shows different implications for the stability of the surrounding ground. For example, longwall mining involves the extraction of a continuous coal seam, often resulting in subsidence. Room and pillar mining, on the other hand, leaves pillars of unmined material to support the roof and reduce subsidence.

Mining methods that involve leaving pillars of unmined material to support the roof, pillar failure can contribute to ground deformation (Babanouri *et al.*, 2023) and if these pillars are not designed or maintained properly, they may collapse leading to subsidence and deformation in the overlying ground.

*e) Water Infiltration and Changes in Water Table*

Changes in the water content of the rock mass can influence ground deformation. Water infiltration into mined areas can alter the mechanical properties of the rock, potentially leading to instability (Yan *et al.*, 2020). Moreover, changes in the water table, either due to mining activities or natural variations, can impact ground deformation (Zhao & Konietzky, 2020; Shizhong Zhang *et al.*, 2021).

*f) Inadequate Support Systems*

Rockfall incidents in mines continue to occur, as alluded to by Molinda and Mark (2010). Investigating the six common types of underground roof falls in coal mines. They discovered that the design and use of support systems in underground mines, such as rock bolts, mesh, and other ground reinforcement methods, are critical in preventing ground deformation, and thorough consideration for surface controls is indispensable. Ghorbani *et al.*, (2020), reviews various support systems in high-stress underground mining settings, discussing how inadequate support can lead to collapses, subsidence, and other forms of deformation. Using practical examples, they provide mitigation measures in burst-prone ground conditions.

## 2.5 Underground rock deformation structures

The Kentucky Geological Survey (2019), describes the types and characteristics of displaced rock masses in an underground mine. The boulder formations (Figure 3) follow

a result of weathered rocks, which occur when water and other environmental conditions cause the rock to weather and disintegrate from the surrounding rock. This change causes an area of weakness and results in instability, making this boulder susceptible to deformation as a result of internal rock stress and gravity (Dan et al., 2016).

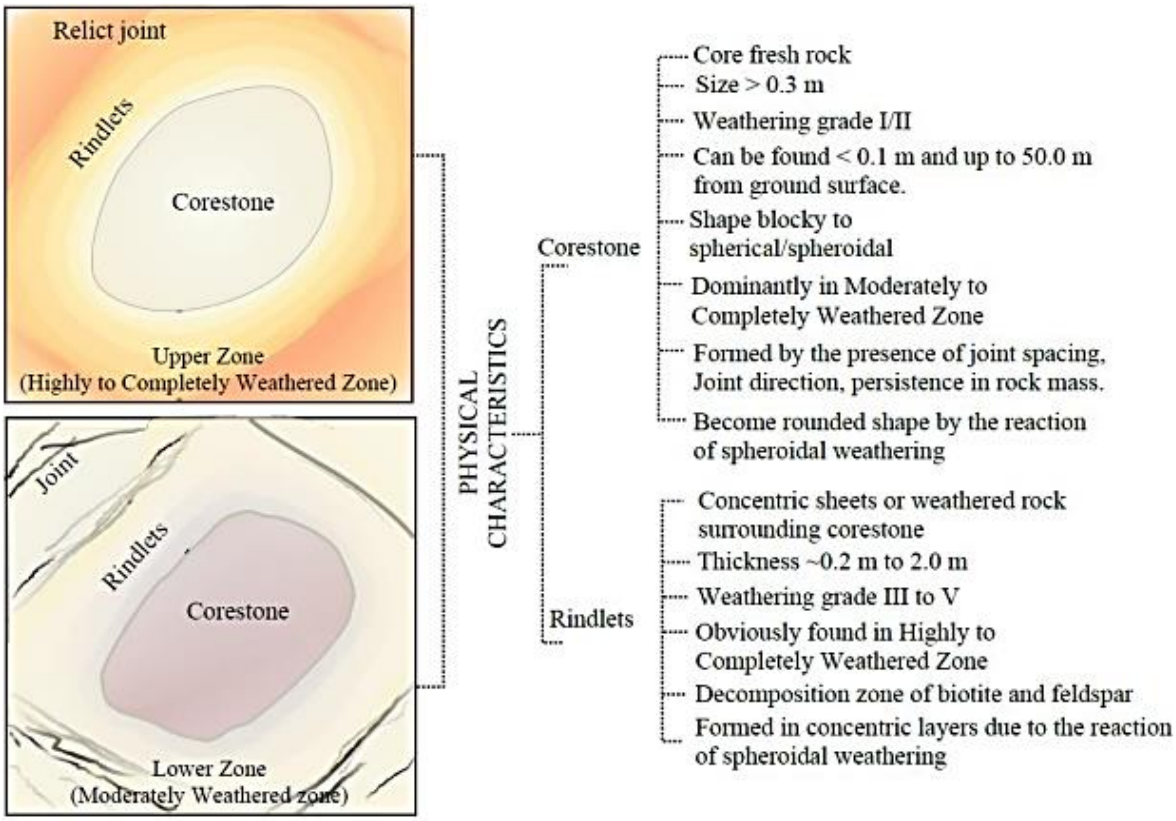



Figure 3: Summarization of the occurrence and characteristics boulder weathered rock mass (M. Dan *et al.*, 2016)

**a) Kettlebottom Roof failure simulation**

Lightweight materials were chosen so to imitate the Kettlebotom formations. The suspended formations were simulated using plastic bags filled with paper; this enabled the shape of the desired deformation, and because of the material's lightweight, it was possible to suspend the formation from the roof of the tunnel without changing its shape and distorting the measurements, as shown by Figure 4.

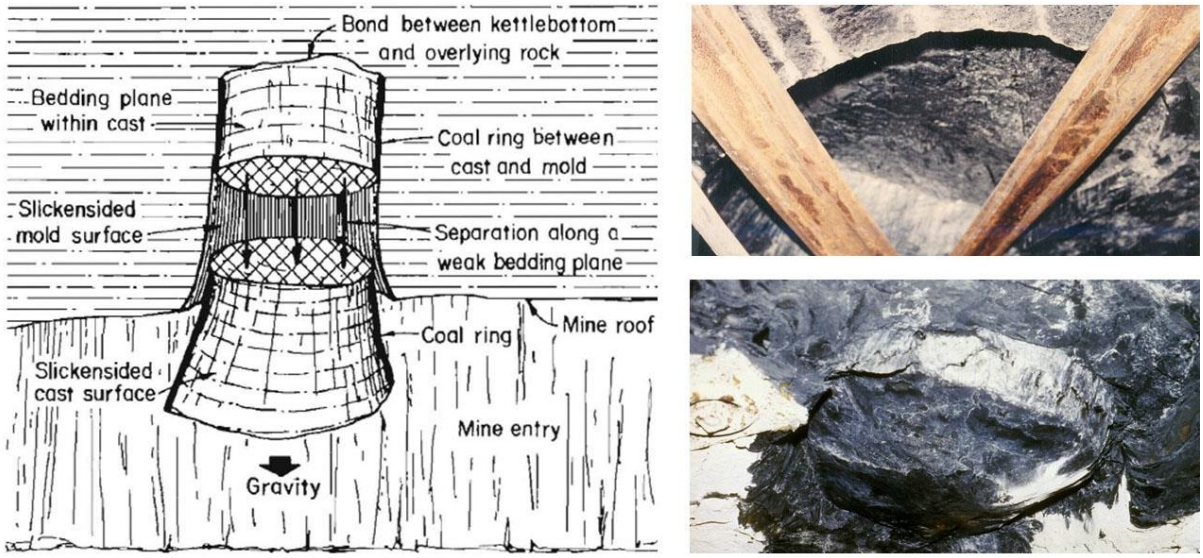



Figure 4: Isolated semi-circular rock mass in a mine roof. With a rounded or flat bottom when viewed from below (Kentucky Geological Survey, (2019))

**b) Cavern sidewall deformation simulation**

Rock displacement includes the movement of rocks inward or outward (bulging) from their original position, as shown in Figure 5 and Figure 6. This displacement results from rock stress release moving the rock from an area of high stress to low stress. When this rock movement occurs and there is no elasticity in the rock, the rock may be ejected as it deforms this is a rock burst phenomenon (Figure 7) (Deng *et al.*, 2019).

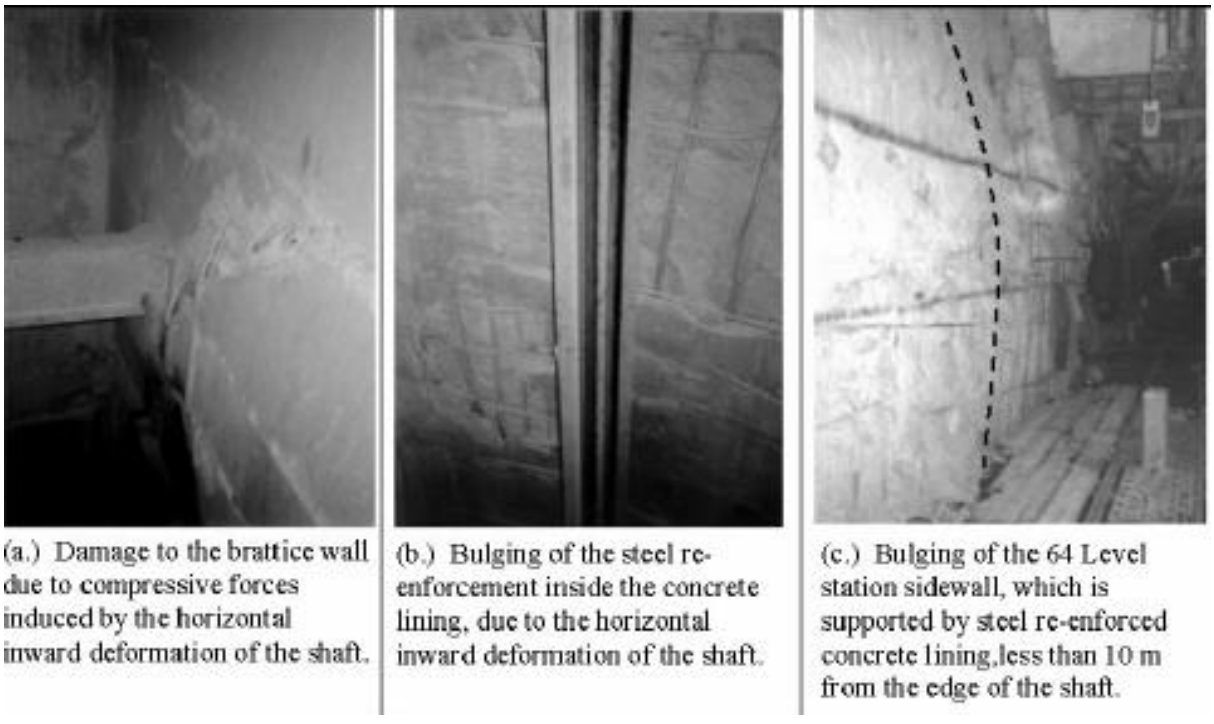



Figure 5: Observed damage to the brattice wall, shaft concrete lining and the sidewall of the 64 Level station (Judeel, 2003).

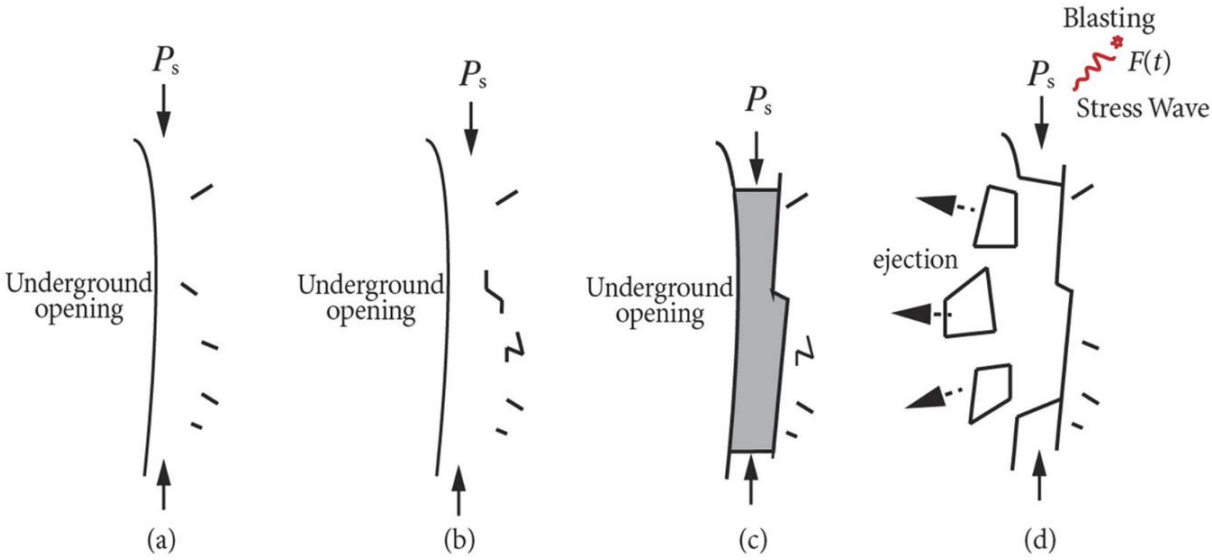



Figure 6: Development of rockbursts on rock surface: (a) Surface of an opening, (b) growing cracks, (c) A slab, and (d) Buckling (Deng et al., 2019).

### 2.6 Risk and Hazards in Underground Mines

The primary risks associated with rock deformation is the potential for rock falls or roof collapses (Zhao *et al.*, 2023). Deformation can lead to rock mass instability and fractures, which compromises the structural integrity of tunnels and shafts increasing the likelihood of sudden failure (Monika *et al.*, 2023). This is very dangerous in underground mines because workers and equipment are in the closest proximity to the enclosing rock. Deformation can induce seismic events caused by the sudden violent release of accumulated stress, water and toxic gasses within the rock (Rahimi *et al.*, 2020; Wu, 2021). These catastrophic events cause damage and are a serious safety risk to miners, infrastructure, and mining equipment such as conveyor belts, support structures and ventilation systems, inherently disrupting mining operations.

Sudden failures do not only affect the miners and mining equipment, but above ground subsidence can damage buildings, roads and other infrastructure (Pawluszek-Filipiak & Borkowski, 2021). Moreover, ground subsidence has environmental impacts such as contamination of water sources or disruption of ecosystems. These drastic changes negatively affect communities near the mining operation, putting their health and property at risk.

## 2.7 Importance of underground Deformation monitoring

Perhaps the foremost importance of underground deformation monitoring lies in ensuring the safety of personnel working in underground mines. Understanding and managing the complex causes of ground deformation as highlighted in previous sections, requires a multidisciplinary approach that integrates geological knowledge, advanced monitoring technologies, and engineering expertise (Bazaluk *et al.*, 2022).

The underground environment is dynamic, and deformations can signal potential hazards such as ground subsidence, roof collapses, or wall failures (Zeng *et al.*, 2020). Monitoring allows for the early detection of these deformations, enabling mining operators to implement timely evacuation procedures and safety measures, thereby reducing the risk of accidents and injuries (Singh *et al.*, 2023).

Because underground mines are supported by a network of tunnels, shafts, pillars, and other structures (Wagner, 2019). Monitoring deformations assesses the structural integrity of these components (Kavvadas, 2003; Małkowski *et al.*, 2020; Monika *et al.*, 2023; Wang *et al.*, 2023). Operators can make informed decisions regarding structural reinforcements, ensuring the stability and longevity of the underground infrastructure (Molinda & Mark, 2010). Deformation data provides valuable information for optimising ground support systems within the mine. Whether it's the installation of rock bolts, mesh, or other reinforcement measures, monitoring helps in understanding the effectiveness of these support systems. Adjustments can then be made to enhance the overall stability of the underground environment.

Efficient mining operations depend on stable and predictable conditions (Chaulya & Prasad, 2016). Changes in the subsurface can impact the orientation and accessibility of ore bodies and monitoring allows for adaptive mining strategies, optimising resource extraction (Khan *et al.*, 2022). Whether it's the gradual movement of rock masses or sudden shifts in the subsurface, monitoring systems can detect these changes. Early detection allows mining operators to take pre-emptive measures, mitigating the impact of hazards and preventing catastrophic events (Kumar, 2010), such as collapses or rockfalls.

Mining activities, particularly in environmentally sensitive areas, can adversely affect the surroundings. Deformation monitoring helps mitigate these impacts by identifying potential risks to the environment. For instance, ground subsidence can affect surface water flow (Newman *et. al*, 2017), and monitoring systems can provide data to implement measures that minimise environmental disturbances, protecting ecosystems and water resources (Council National Research *et. al*, 2011).

Many mining operations are subject to strict regulatory standards, such as the South African MPRDA Act, 28 of 2002 and the Mine Health and Safety Act No. 29 of 1996, regarding safety, environmental impact, and structural stability. Implementing deformation monitoring systems ensures compliance with these regulations (Onifade *et al.*, 2024). It also demonstrates a commitment to responsible mining practices, reducing the likelihood of accidents and environmental damage, and helps mining operations adhere to legal requirements (Ratsheko, 2018).

## 2.8 Monitoring underground deformation using different technologies

Mining activities can have adverse environmental consequences, and monitoring helps mitigate these impacts. Proactive measures can then be taken to minimise these effects (Brink *et al.*, 2008; Małkowski *et al.*, 2020). Traditional ground-based techniques involve listening for cracking sounds of rocks or visual assessment for identifying unstable rock conditions and installing surveying instruments within the mine. These instruments, such as total stations and inclinometers, measure movements in specific locations (Salcher, 2015). While accurate, these methods may have limitations regarding coverage and real-time monitoring capabilities. Advanced technologies like satellite-based remote sensing and LiDAR (Light Detection and Ranging) are increasingly being employed for deformation monitoring (Duarte *et al.*, 2022; Singh *et al.*, 2023). These techniques offer broader coverage and can provide near-real-time data on deformations. They are particularly useful in large-scale mining operations where traditional ground-based monitoring may be impractical (M. Wang *et al.*, 2020; Bazaluk *et al.*, 2022).

### 2.8.1 Ground-Based Monitoring Instruments

Strain Gauges: Strain gauges measure the amount of changes in strain or deformation of materials. These devices can be installed on structural elements within the mine to

monitor changes in their shape or size (Iskander, 2018). For example, gauges can be bonded on rock bolts, pillars, or tunnel walls. As the material undergoes deformation, the strain gauge detects changes in resistance and provides quantitative data on the magnitude and direction of the deformation.

Inclinometers: These are instruments used to measure the inclination or slope or tilt of a surface. They are placed on tunnel walls or pillars to detect any inclination changes, providing valuable data on ground movements or deformations (Iskander, 2018).

Load Cells: These sensors measure the force or load applied to a structure. In mining, load cells can be integrated into support systems such as rock bolts or pillars to monitor the load-bearing capacity and detect changes in the forces acting on these structures (Iskander, 2018). Sudden load increases may indicate potential instability.

Tiltmeters: Measure the tilting or rotation of a surface. These devices are useful for detecting angular deformations in underground structures (Iskander, 2018). Tiltmeters are often employed in areas where changes in the orientation of rock masses or pillars may indicate impending structural issues.

Pressure Cells: Instruments used to measure changes in pressure within a material. They are installed in the rock mass or support structures to monitor changes in stress distribution. Sudden variations in pressure may indicate potential deformation or instability (Jacobs, 2016).

Vibrating Wire Sensors: Vibrating wire sensors are versatile instruments that can measure various parameters, including strain and displacement (Zare *et al.*, 2021). In underground deformation monitoring, these sensors are often embedded in boreholes or attached to structural elements. The vibrating wire technology provides precise and stable measurements, even in challenging underground environments (Gokhan & Korkut, 2013).

Crack Meters: Monitor the opening or closing of cracks in rocks or structures, especially in areas with potential subsidence or stress-induced cracking (Benton *et al.*, 2016). The instruments are used to assess the development of fractures and evaluate the impact on structural integrity.

Extensometers: In underground mining, extensometers are commonly used to monitor the displacement of rock masses or structural elements (Salcher, 2015). These devices can be installed between two reference points, providing continuous measurements of strain and allowing for the assessment of deformation patterns. These measurements are done daily until the disturbed rock mass movement is stabilised (Delaloye, 2012). Some extensometers, like the tape-extensometer, disturb tunnel construction progressions because they must be permanently mounted on the rock walls. Their accuracies and precision are easily compromised by the monitoring system installation and operators, and unfortunately, because the measurement is between two points, asymmetric deformation patterns can be easily missed (Yang *et al.*, 2017b). Inadequate information on the geotechnical conditions of the host rock is one of many reasons calamities in underground mines continue to compromise human health and safety (Hebblewhite, 2019).

### 2.8.2 Remote Sensing-Based Deformation Monitoring Methods

*Geodetic Method*

The geodetic method involves the use of precise positioning techniques, such as Global Navigation Satellite Systems (GNSS) and total stations, to measure the coordinates of specific points on the Earth's surface (Jing-xiang & Hong, 2009). Geodetic methods are employed to monitor surface deformation and subsidence in underground mines. GNSS receivers can be placed on the surface (Zare *et al.*, 2021). Total stations provide accurate measurements of specific points within the mine, contributing to a comprehensive understanding of ground movements.

*Total Stations*

Total stations are the most basic geodetic instruments that measure angles and distances with high accuracy and precision (Braunová *et al.*, 2023). In underground mining, total stations can be strategically placed to monitor specific points for deformation (Leica Geosystems, 2019). They seem effective for localised monitoring but may have limitations in terms of coverage and accessibility in complex underground environments. There have, therefore, been integrations to produce automated total stations, such as demonstrated by Braunová *et al.* (2023), when they used robotic total stations, which combine the precision of traditional total stations with automation

features. These instruments can be programmed to monitor specific points at regular intervals, providing continuous and accurate deformation data on surface and underground mines.

*Global Navigation Satellite Systems (GNSS)*

GNSS, including GPS (Global Positioning System), can be utilised for deformation monitoring (Jing-xiang & Hong, 2009). GNSS receivers placed on the surface or integrated into the mine infrastructure can track the movement of specific points over time. However, direct underground GNSS monitoring can be challenging due to signal attenuation (Singh, Banerjee, *et al.*, 2021).

### 2.8.3 Wireless Sensor Networks (WSNs)

WSNs consist of distributed sensors strategically placed throughout the underground mine (Zare *et al.*, 2021). These sensors collect data on deformation and transmit it to a centralised system. WSNs offer real-time monitoring capabilities, allowing for continuous assessment of subsurface conditions over a broad area (Atif *et al.*, 2021; Sadeghi *et al.*, 2022).

Seismic sensors, as an example of WSNs, involve the measurement of ground vibrations caused by subsurface movements or seismic events (Gokhan & Korkut, 2013). Measured by an array of seismic sensors, often known as geophones, deployed across the surface, they provide information about the subsurface structure and potential surface deformations (Garré *et al.*, 2023). In underground mining, seismic methods are employed to monitor rock mass behaviour, detect fractures, and assess the impact of mining activities on the surrounding geology (de Santis *et al.*, 2019). They are particularly useful for identifying potential areas of instability.

### 2.8.4 Fiber Optic Sensors

Fibre Optic Sensors are increasingly employed for deformation monitoring in underground mines. Distributed Fiber Optic Sensing (DFOS) systems use optical fibers installed along mine structures to detect changes in strain or temperature (Gong *et al.*, 2019). This technology provides continuous and real-time monitoring over long distances. Fibre DFOS have been tested in a deep mining environment to monitor strain characteristics at multiple measuring points and showed they can be synthesised to

effectively determine the development height of the caving and fissure zones in roofs (Xu *et al.*, 2015).

### 2.8.5 Radar-Based Monitoring

Ground-penetrating radar (GPR) is used for subsurface monitoring. GPR sends electromagnetic waves into the ground and measures the reflected signals, allowing for the detection of changes in material properties and potential subsurface deformations (Wang *et al.*, 2012). This method has been applied in underground karst mines for karst void detection before mining (Baggett *et al.*, 2020). Weidong et al. (2012) demonstrate with a 100-MHz system the detection of loose rock as a result of blasting, fragmented rock 18 m behind the working face, and fissure water (Weidong *et al.*, 2012). Wang et al. conducted a GPR survey on the walls of a tunnel to detect vertical shafts successfully (Wang *et al.*, 2012). These studies prove the capabilities of GPR as a monitoring and investigative instrument in underground excavations.

*a) InSAR (Interferometric Synthetic Aperture Radar)*

InSAR uses radar images captured by satellites to detect millimetre-scale ground movements by comparing phase differences between radar images acquired at different times. In underground mining, InSAR can be used to monitor surface subsidence and detect deformations in areas within the reach of radar signals, such as open pits or partially covered areas (Ng *et al.*, 2011).

*b) DInSAR (Differential Interferometric Synthetic Aperture Radar):*

DInSAR is an advanced form of InSAR that provides even higher accuracy by comparing pairs of SAR images acquired at different times (Jiang *et al.*, 2023). It is useful for detecting small-scale deformations (Monika *et al.*, 2023) and changes in the terrain (Pawluszek-Filipiak & Borkowski, 2021), which can be critical for monitoring underground mining activities and their impact on surface stability.

### 2.8.6 Internet of Things (IoT)

IoT-based deformation monitoring involves the deployment of interconnected sensors and devices in the underground environment (W.-H. Zhou *et al.*, 2024). These sensors collect data on various parameters such as strain, temperature, and pressure, transmitting the information to a centralised system (Atif *et al.*, 2021). This enables real-time monitoring of subsurface conditions, allowing for early detection of deformations. In Figure 7, Hao et al.,(2020), illustrates how the interconnected nature of IoT devices facilitates a comprehensive understanding of the underground environment and enhances the responsiveness to potential risks.

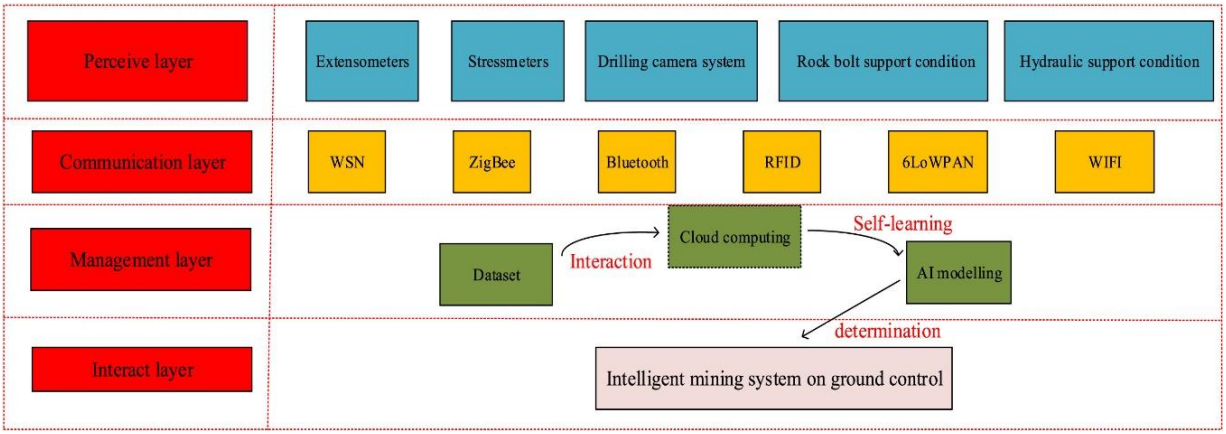



Figure 7: The framework of ground control with IoT in underground coal mines (Hao et al., 2020)

Advanced software solutions are used to process and analyse data from various monitoring technologies to derive actionable, context-aware applications (Mohindru *et al.*, 2020). Data analytics, machine learning, and artificial intelligence techniques are often applied to this data to identify patterns, predict potential hazards, and optimise mining operations based on historical data (Mohindru *et al.*, 2020; Atif *et al.*, 2021). These tools create 3D models of the underground environment, allowing mining engineers to visualise and interpret deformation patterns (Hao *et al.*, 2020).

### 2.8.7 Optical Methods

Optical methods, including drone technology, utilise cameras and sensors to capture high-resolution images and data (Walker, 2023). Drones can be equipped with visible, infrared, or thermal cameras to monitor surface features and detect changes over time (Broere, 2024). In underground mining, drones are employed for mapping and monitoring surface features, such as sinkholes or subsidence (Pawlik *et al.*, 2024) . They provide a

cost-effective and flexible solution for obtaining detailed images of inaccessible or hazardous areas, aiding in deformation assessment and risk mitigation.

A common example is close-range photogrammetry, as detailed by Benton et al., (2016) is a powerful, quick and easy way to capture underground rock surface geometry and detect changes and hazardous conditions. This technique derives the shape of an object in 2D and 3D from the measurement of multiple high-resolution images; it is considered a fast, cheaper and more precise supplement in contrast to extensometers and other in situ methods (Slaker & Mohamed, 2017). But photogrammetry is not without limitations in the underground space; low lighting and uneven wall surfaces, which impact the quality of its surveys, make it a less popular technique. In (2019)Bishop et al. compared the use of photogrammetry to the newly emerged LiDAR laser scanning in an underground limestone mine. Their findings showed laser scanning to have more advantages to photogrammetry, especially in large-scale surveys.

### 2.8.8 Light Detection and Ranging (LiDAR)

LiDAR technology uses laser beams to measure distances and create detailed 3D geomatic maps of the underground environment (Singh, Banerjee and Raval, 2021). The laser scanning, also called Light Detection and Ranging (LiDAR) surveying technique, does not only assesses geometrical states but has evolved to assess changes in those specific states and records them in millions of points, each point with longitude, latitude and elevation (x, y, z) (Uggla & Horemuz, 2021). Light detection and ranging measures the distance from the laser scanner to the area in the device's field of view (Lindenbergh & Pietrzyk, 2015a). Because collapses start with small movements before the final catastrophe, multiple scans from different epochs and positions from a moving tunnel face can be compared over time to form a tunnel profile (Gikas, 2012a). Information extracted from the profiles can be used to identify and quantify changes between point clouds at different times (Jia *et al.,* 2021). This principle has been successfully demonstrated in studies monitoring rock deformation and movement (Slaker, 2015; Alzahrani, 2017; Yang *et al.*, 2017a). Pinpin *et al.* (2021) highlight the shortcomings of tunnel overbreak and underbreak detection using in situ methods and suggest the use of three-dimensional laser technology to overcome the inefficiencies (large workload, a small number of points, low accuracy, and poor efficiency). They compared LiDAR

measurements to total station measurement results and found laser scanning a detailed, accurate and reliable detection method.

Unlike in situ methods with limited coverage, laser scanning captures the entire geometric detail of a surface in the horizontal and vertical (van der Merwe & Andersen, 2013a), this would be the entire length of the tunnel instead of specific sections at meter intervals. This extensive amount of data requires computationally efficient feature extraction methods for processing and interpolating errors acquired from one epoch of a scene to another (Romero *et al.*, 2016), also allowing for the extraction of any section of the tunnel to be studied (Wang, H. B. Zheng, *et al.*, 2017). Laser scanning metiers also include the acquisition of a large number of single points of a scene in a short stint, a substantial advantage in mining survey: it is quick, does not require illumination to capture data, and the point clouds enable the removal of noise such as dust and equipment (Zlot & Bosse, 2014b; Webber-Youngman et al., 2019).

Studies done in underground mining have shown the applicability of LiDAR technology to be utilised for mapping tunnels, shafts, and other structures (Broere, 2024). Woolmer *et al.* (2020), Studied the incorporation of LiDAR remote sensing-based deformation monitoring methods into the Olympic Dam underground mining operation to enhance their ability to access accurate stope survey data for managing risk and planning outputs. Their findings attest to LiDAR's accurate and high-density spatial data output, enabling the assessment of deformation patterns and the identification of potential hazards (Woolmer et al., 2020).

The growing use of terrestrial laser scanners in mining has been fuelled by the need to produce contemporaneous, accurate and precise geotechnical data due to the progressive and rapidly changing nature of the mining environment (van der Merwe & Andersen, 2013a). The TLS's precision and accuracy enable miners to conduct surveys that are essential for monitoring the rapid, complex, volatile rock-enclosed environment. The point cloud collected in conjunction with related information removes the calamity of blind-mining and allows managers to make informed decisions that improve health and safety in the mining space (Lindenbergh & Pietrzyk, 2015a).

Although the static laser scanning approach for underground mapping and monitoring is lavished with benefits, the limitation of the existing method is the instrument's heavy weight, a high number of working stations, and the significant amount of time needed for scanning (Elisa Mariarosaria Farella, 2016). But fortunately, as a common trait of technology, lighter, faster instruments are being developed, such as the backpack and handheld mobile LiDAR scanners. Mobile LiDAR systems can also be mounted on vehicles or drones to rapidly scan and monitor large underground areas (Woolmer *et al.*, 2020), providing high-resolution data for deformation analysis (E. Jones, 2020)

Table 2: Comparison of underground rock deformation monitoring methods, their applications, advantages and disadvantages.

| **Monitoring Method** | **Applications** | **Advantages** | **Disadvantages** |
|---|---|---|---|
| **InSitu Methods** (Slaker, 2015; Iskander, 2018) | • Monitoring structural elements, rock bolts, and tunnel deformations<br>• Assessing localised ground movements | • High precision and accuracy<br>• Real-time monitoring capabilities<br>• Direct measurement of local deformations<br>• Suitable for detailed analysis of structural elements | • Limited coverage compared to remote sensing methods<br>• Requires physical installation in the underground<br>• May be challenging to install in inaccessible areas |
| **Seismic Methods** (Gokhan & Korkut, 2013; de Santis *et al.*, 2019) | • Assessing rock mass behaviour and seismic risk<br>• Early warning of seismic events | • Detects potential ground instability<br>• Provides information on subsurface structures | • Requires specialised equipment and expertise<br>• High initial setup costs |

| | | | |
|---|---|---|---|
| | | • Can be used for early warning of seismic events<br>• Suitable for assessing rock mass behaviour | • Limited to detecting large-scale movements |
| **IoT Methods** (Atif *et al.*, 2021; W.-H. Zhou *et al.*, 2024) | • Monitoring various parameters (strain, temperature, pressure)<br>• Integration for holistic analysis<br>• Flexibility in deployment and scalability | • Real-time data collection and transmission<br>• Comprehensive monitoring of various parameters<br>• Enables data integration for holistic analysis<br>• Flexibility in deployment and scalability | • Dependence on network connectivity<br>• Initial setup costs for sensor deployment<br>• Potential for sensor malfunctions and data errors |
| **Optical Methods (Drones)** (Benton *et al.*, 2016; Walker, 2023) | • Rapid assessment of surface deformations<br>• Monitoring changes in surface topography | • High-resolution imaging of surface features<br>• Flexibility in reaching inaccessible areas<br>• Cost-effective compared to traditional methods<br>• Rapid data collection over large areas | • Limited to surface monitoring<br>• Environmental conditions (lighting, dust, weather) dependent operations<br>• Limited payload capacity for advanced sensors |

| | | | |
|---|---|---|---|
| **Laser Scanning, InSAR, DInSAR** (Wang *et al.*, 2012; Monika *et al.*, 2023) | • Identifying subtle ground movements | • High precision and accuracy<br>• Provides detailed 3D models of structures<br>• Enables the detection of subtle ground movements | • Limited to surface or near-surface monitoring<br>• Costs associated with data processing and analysis<br>• Affected by atmospheric conditions |
| **Geodetic Methods** (Jing-xiang & Hong, 2009; Braunová *et al.*, 2023) | • Monitoring surface deformation due to mining activities<br>• Commonly used in conjunction with other methods | • High precision in measuring coordinates<br>• Provides accurate spatial information<br>• Suitable for monitoring surface deformation<br>• Commonly used in conjunction with other methods | • Limited to surface monitoring<br>• May be affected by atmospheric conditions<br>• Requires clear line-of-sight for GNSS<br>• Setup and equipment costs |
| **LiDAR (Terrestrial, Mobile)** (Lindenbergh and Pietrzyk, 2015a; Pinpin et al., 2021) | • Mapping tunnels, shafts, and structures<br>• Identifying deformation patterns in underground structures | • Provides accurate and high-density spatial data<br>• Suitable for mapping tunnels and structures<br>• Rapid data collection over large areas | • High initial setup and equipment costs<br>• Limited by line-of-sight, may not penetrate obstacles<br>• Requires skilled personnel for data processing |

| | | | |
|---|---|---|---|
| | | • Valuable for identifying deformation patterns | |

As detailed in the preceding sections and summarised in Table 2, various technologies are employed for deformation monitoring, each offering distinct advantages in terms of accuracy, coverage, and real-time capabilities. The choice of technology depends on factors such as the specific requirements of the mining operation, the geological conditions, and the desired level of monitoring precision. LiDAR remote sensing technology emerges as the most robust, detailed and efficient, especially in extensive, complex underground mining environments.

### 2.9 Working principles of LiDAR remote sensing

Light detection and ranging (LiDAR) is an active remote sensing method used to examine the Earth's surface at high resolution (Carter *et al.*, 2012). The system uses laser beam projection, and the sensors measure the time it takes for the laser to reflect back from a target object to the sensors (Padmanabhan *et al.,* 2019). It uses light in a pulsed laser form to measure numerous point distances to the target, which collectively are referred to as a point cloud and also detect the energy reflected by these numerous surface points. As the laser is pointed at a target, a continuous beam of light is emitted towards it and reflected by the object. The light pulses produce meticulous three-dimensional data about the target, and this data can give us the shape and surface characteristics of the surrounding (Li et al., 2020; Singh et al., 2021).

LiDAR instruments are principally made up of a laser, a scanner and, in other cases, a GPS receiver and a digital single-lens reflex camera (DSLR), which helps display the point cloud data in RGB colours. There are two forms of LiDAR available: bathymetric LiDAR, which uses water-penetrating green light and topographic LiDAR, commonly referred to as terrestrial LiDAR, which uses near-infrared laser (900nm – 1064nm) of the electromagnetic spectrum to capture details of the land (Quadros *et al.,* 2008). Terrestrial laser scanners comprise three categories: short (triangulation laser

scanners), medium (phase shift) and long-range scanners (time-of-flight), subject to the distance the laser light can travel to record data of points within its field of view (Fröhlich & Mettenleiter, 2004). Short-range scanners measure areas in high detail and accuracy, but are limited to only a few meters, and the interval between adjacent points may be 1 millimetre (Schulz & Ingensand, 2004). Contrary to short-range scanners, long-range scanners have been optimised to measure up to hundreds of kilometres, an advantage for spatially extensive areas (Suchocki, 2020). TLS can be classified in several ways, but the most widely used in published literature is the distance measurement technique. The major sensor techniques for this method, as detailed by Suh (2019), are optical triangulation, interferometry and time-of-flight sensors.

Triangulation works based on a laser light and a detector. A light source scans the target, and the reflected signal is picked up by the detector, which is recorded by an optical sensor. This method's accuracy is precise up to a few meters (Idrobo-Pizo *et. al*, 2019) and is also affected by temperature (Kuester *et al.,* 2018). It is therefore not suitable for surveying.

Interferometry is an ultra-precise measurement technology that can measure nanometre-range displacements over very short distances. This method is founded on the interference of light beams, where two light or laser beams are propagated to a target and a reference mirror, producing an interference pattern with light intensity variations (Sirohi, 2018). This pattern is analysed to measure physical quantities, such as the distance, displacement, and velocity (Wang & Fang, 2017).

The Time-of-flight method measures the time a beam takes to travel from its source to a target by sending a narrow laser beam and recording the received reflected signal. Time-of-flight has two operating principles for measuring distance. The first approach is pulsed time-of-flight, also known as direct time-of-flight, where a short pulse is used to measure the time elapse between signal emission and its return to the sensor (Padmanabhan *et.al*, 2019). From this measurement, a 3D polar coordinate is calculated using the horizontal and vertical angles recorded in the apparatus (Lin *et al*, 2020). Contrastingly, indirect time-of-flight or phase shift relies on the phase difference between the transmitted continuous modulated light and its reflected signal. A (2020) study by Wang

*et al.* compares the two operating principles for LiDAR scans; they conclude that time-of-flight methods have a maximum measurement range advantage over phase shift, notwithstanding that phase shift has higher acquisition speed and accuracy. Pulse-based systems are generally applied for surveying, whilst phase-based scanners are utilised for mapping small environments.

The growing use of terrestrial laser scanners in underground mining has been fuelled by the need to produce contemporaneous, accurate and precise geotechnical data due to the progressive and rapidly changing nature of the underground mining environment (van der Merwe & Andersen, 2013b). The TLS's precision and accuracy enable miners to conduct surveys that are essential for monitoring the rapid, complex, and volatile rock-enclosed environment. The point cloud collected in conjunction with related information removes the calamity of blind-mining and allows managers to make informed decisions that improve health and safety in the mining space (Lindenbergh & Pietrzyk, 2015b).

Although the TLS approach for underground mapping and monitoring is lavished with benefits, the limitation of the existing methods is the instrument's heavy weight. But fortunately, as a common trait of technology, lighter instruments are being developed.

### 2.9.1 LiDAR platforms and their working principle

LiDAR sensors are mounted on different platforms, giving the technology versatile access to especially restricted areas like underground environments with high safety risks. LiDARs are mounted on static ground-based platforms such as tripod-stands, mobile platforms such as human-carried and cars, and finally, airborne LiDAR mounted on aeroplanes and recently AUVs. Several studies have been conducted to demonstrate the efficiency and benefits of the application of LiDAR on the various platforms. In 2012, Delaloye used a static laser scanner to measure the deformation of underground tunnels and shafts. Lindenbergh and Pietrzyk (2015) used the static and vehicle-mounted mobile LiDAR for change detection, Singh *et. al.* (2021) used mobile laser scanning for classifying and mapping roof bolt density and spacing of an underground coal mine, and Dewez *et. al.* (2017) gathered geometric details of mine cavities and mapped collapse hazard localities using a handheld mobile laser scanner. The static laser scanning

systems' ease of control limitations have given mobile LiDAR preference as a more compact and rapid data acquisition platform (Thomson *et al.*, 2013).

### 2.9.2 Terrestrial Laser Scanning

TLS are ground-based scanning instruments and, depending on the nature of use, can be connected to a moving vehicle or mounted on a tripod. In a (2018) study by Vazaios *et al.*, a tripod platform was employed to provide detailed surface geometry, whilst Russell and Stacey (2019) highlight the use of a vehicle-mounted TLS for geotechnical face mapping as needed, mentioning the need to stop-and-go the scanner vehicle during the scanning process. Static Lidars rely on repetitive slope measurements rapidly acquired at known angular intervals by an Electric Distance Measurer (EDM) (Gikas, 2012b). The angles are defined in the horizontal and vertical of the EDM passing through the sensor's origin (Mariusz & Zbigniew, 2014). This process generates points in spherical polar coordinates (radius $r$, elevation $\omega$, azimuth $\alpha$, presented x,y,z) of the scanner's field of view (Morales *et al.*, 2018). Scanning in this method can be done in one of two ways: single scanning or multiple scanning. Single scanning involves placing the scan in one position producing a single dimension of the scanned object. Whilst the multi-scanning method entails scanning from 3 or 4 different positions about the object or area of interest, allowing for a single object to be scanned in different directions (Ritter *et al.*, 2020).

### 2.9.3 Terrestrial mobile laser scanning

Terrestrial mobile or kinematic laser scanning technology is a point cloud acquisition method that is mounted on mobile platforms such as cars and boats and has been suited for large-scale outdoor scanning, limiting its use in indoor spaces because of its reliance on Global Navigation Satellite System (GNSS). But the development of the SLAM (simultaneous localisation and mapping) algorithm as detailed by Zlot and Bosse (2014a), an alternative approach which is able to construct a map of an unknown surroundings while simultaneously keeping track of its trajectory (Keitaanniemi *et al.*, 2021). This is the a parallel integration of LiDAR records with inertial measurement units (IMU) data, which detects the spatial movement of the instrument, has enabled underground mining surveys using mobile scanning (Wajs *et al.*, 2018). SLAM-based software have opened a realm of possibilities leading to advancements in the mapping of underground mines, especially large-scale underground mines because it is a

challenging and timeous venture. Dewez *et al*., (2017) mapped cavity collapse hazards using a mobile scanner. Singh *et al.,* (2021) used mobile LiDAR to create 3D map for identifying roof bolts.

### 2.10 Georeferencing methods for terrestrial LiDAR Scanning

When capturing the geometric information of the underground site, it is generally required to have multiple aspects of the area of interest. Thereafter, geometric alignment or georeferencing of the different data sets into a shared reference frame is crucial. When measurements are georeferenced, basic sensor datasets become geodata, and this allows for combination with other geodata. The sooner the data is georeferenced, the earlier data completeness, coverage and other quality factors can be checked in the field in relation to existing geodata (Schuhmacher & Böhm, 2005).

#### 2.10.1 Conventional Georeferencing Approach

Conventionally, registration and georeferencing are conducted simultaneously. The common requirement for georeferencing terrestrial laser scan data using the conventional approach is at least three known 3D tie-points in each scan. These are provided by 3 targets, and because these 3D control points do not occur naturally, to incorporate height and position, a supporting measurement system, such as a total station, is introduced. And although this process is time-consuming and costly and requires operational knowledge of the second measurement instrument, it is considered the most precise method for assigning a geometric datum to terrestrial laser scanning measurements. Considering this method's cons two common alternatives have been explored for georeferencing to overcome the mentioned shortcomings these are the sensor-driven and data-driven approaches.

### 2.11 Point cloud data management

The applicability and effectiveness of the static and mobile laser scanning technique in improving the monitoring of rock masses relies on the density and quality of the point cloud and the processing technique applied (Gikas, 2012b). Raw point cloud data sets can be used for Visualisation, but deformation analysis requires data pre-processing to establish corresponding relations of the random points from different epochs (Wang,

H.B. Zheng, *et al.*, 2017). The establishment of a suitable geometric model that suits the real tunnel's surface is essential for deformation comparisons.

A procedure for maintaining quality data such as control and geo-referencing, needs to be followed. Static laser scanners require positioning that is accurately surveyed (Zlot & Bosse, 2014a). Whilst in mobile laser scanning, developments such as the occupancy grid method (Artan *et al.*, 2011; Hull, 2017), which replicate the environment by transforming the millions of points into a spatial array with less erroneous results, and the localisation methods for GNSS signal denied areas like the SLAM algorithm (Whyte, 2006; Bosse & Zlot, 2009) which connects 2D laser scanning data and Inertial Measurement Unit (IMU) measurements of the angular velocities and linear acceleration to 3D point cloud (Farella, 2016; Malberg, 2019), have improved mobile mapping. Mobile LiDAR's scan quality and accuracy can be affected by a sensor's range (maximum distance the device can scan), sampling rate (point density, data resolution, moving speed) and ability to assign attributes to each point (Jones, 2020). Jones *et al.*, (2018) fully detail a method for determining accuracy for mobile laser scanning and Kolapo (2020) lays out controls for accuracy testing for static terrestrial laser scanning. Nevertheless, methodical, theoretical and wide aspects of the technique are still being researched (Fekete *et al.,* 2009; Lague *et al.,* 2013; Kang *et al.*, 2014; Xu *et al.,* 2018; Huang *et al.,* 2021) and have not yet been established, however various procedures have been applied that have yielded several progressive developments (Jia *et al.,*2021).

### 2.12 Identified knowledge gap.

The literature demonstrates that deformation monitoring in underground mining has evolved over the years. From conventional in-situ instrumentation, such as strain gauges, inclinometers, and extensometers, to advanced remote sensing techniques, including LiDAR, InSAR, and photogrammetry. LiDAR technology, in particular, has shown considerable promise for high-resolution, three-dimensional mapping of underground environments. However, most existing studies have evaluated static and mobile LiDAR systems independently, often within open-pit mines, surface infrastructure projects, or active underground operations where environmental and operational variability may influence the results.

Few investigations have undertaken controlled side-by-side comparisons of static and mobile LiDAR in identical underground settings. Where comparisons have been made, the focus has largely been on point cloud density, coverage, or cost-effectiveness, with limited emphasis on deformation detection accuracy and operational efficiency under constrained underground conditions. Moreover, studies conducted in real mines often face practical limitations, such as restricted access, safety hazards, and uncontrolled deformation events, which hinder systematic testing.

The use of a mock mine with simulated deformation events, as in this study, offers an opportunity to address these gaps by enabling precise control of experimental conditions while still replicating the spatial and lighting constraints of underground environments. This controlled approach allows for a direct and fair comparison of mobile and static LiDAR performance in detecting and mapping rock deformation within a GIS environment, providing evidence-based insights that are currently underrepresented in academic literature and industry practice.

# Chapter 3

# 3 Methods and Materials

## 3.1 Introduction

This chapter presents the materials and methods utilised to achieve the research objectives. The study investigates rock deformation in an underground mining environment using static and mobile LiDAR systems. The methodology includes the research site details, instruments used, data collection procedures, deformation simulations, data processing workflows, accuracy assessment, and efficiency evaluation techniques. A Total Station was used for georeferencing, and specialised software facilitated point cloud registration, distance calculation, and mesh-to-mesh deformation analysis.

## 3.2 Research Design and Approach

It was important to find a method that would provide accurate displacement measurements so that the slightest significant rock surface movement is accounted for when analysing the LiDAR data (Jafari *et al.*, 2017; Kolapo, 2020). This research utilised a quantitative experimental approach by integrating controlled deformation simulations with high-resolution 3D LiDAR scanning to analyse underground rock displacement. The study's data collection and analysis were structured in two phases outlined in Figures 4 and 5.

### 3.2.1 Displacement Measurement Process: Pre- and post-deformation

Before conducting simulations and conceptualising scanning stations and trajectories, the scanning process was methodically planned and implemented in two distinct phases: pre-deformation (T1) and post-deformation (T2). Establishing a predefined scanning route was essential, especially for mobile LiDAR, as it ensured that the starting and ending points were correctly aligned to form a closed-loop trajectory. This loop helped in error detection, correction, and overall improvement of the data quality during the mapping process (Zlot & Bosse, 2014b).

### a) Pre-Deformation Phase (T1)

The pre-deformation scan (T1) represented the equilibrium state of the tunnel before rock movement occurred. During this phase, scanning was carried out before the deformation simulations were introduced, ensuring that baseline data was collected under stable conditions. Mobile and static LiDAR scans were sequentially performed under the same environmental conditions to ensure consistency and comparability.

### b) Post-Deformation Phase (T2)

Once the pre-deformation scans were completed, simulated deformations representing rock movement-induced changes were implemented. The scanning process (T2) was then repeated along the predefined route using the same LiDAR arrangements as in T1. This ensured that any observed differences between the datasets could be directly attributed to deformation rather than external scanning inconsistencies.

Figure 8 shows the simplified data acquisition process, highlighting the structured method used to measure displacement before and after deformation.

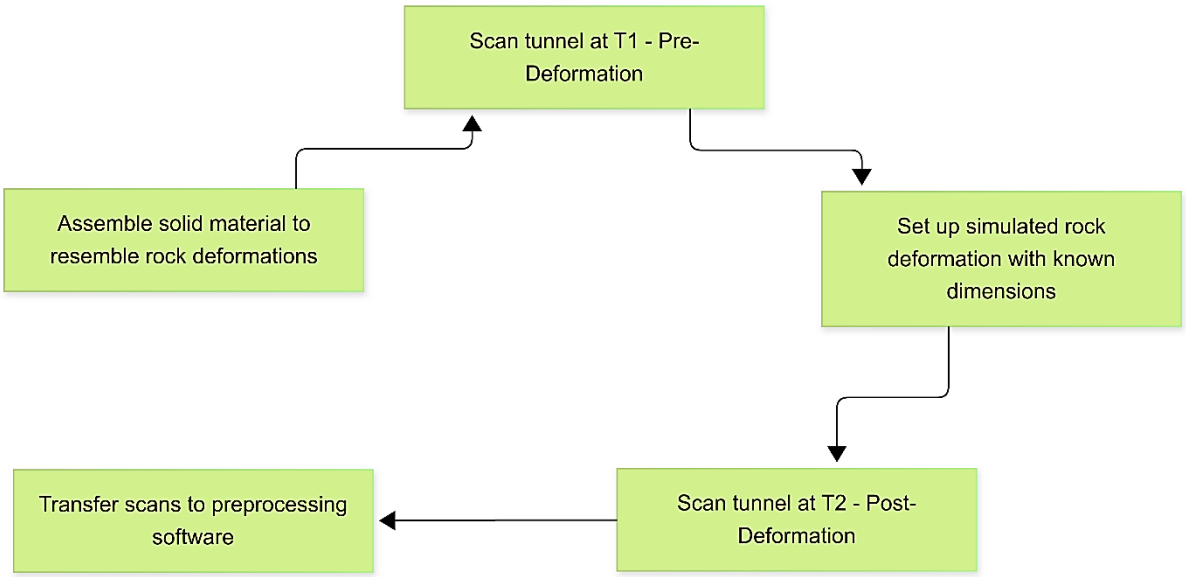



Figure 8: Acquisition process for deformation simulation and measurement.

After capturing the scans, the raw LiDAR data was imported into the processing software and carefully trimmed to isolate the area of interest (Delaloye, 2012). Next, a scan-to-scan comparison (T1 vs. T2) was conducted by meshing each dataset separately to generate surfaces that facilitate precise geometric analysis. The shortest distances between the two surfaces were then computed to detect potential deformations and

changes. Finally, the field data was compared with the LiDAR-derived deformation results to determine which platform—mobile or static LiDAR—produced the most accurate results when validated against ground truth measurements.

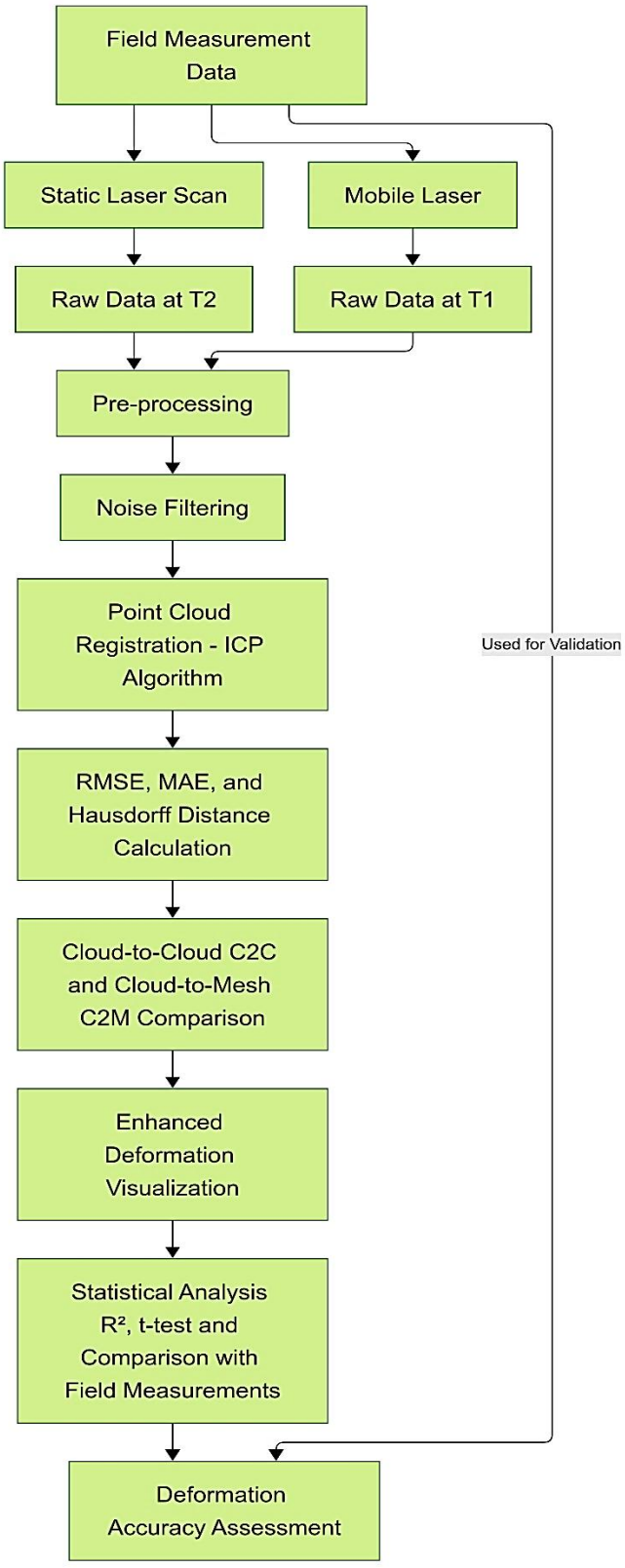



Figure 9: Technical process for calculating deformation based on point cloud data.

The above-mentioned sequences (Figures 8 and 9) were followed to:

- Identify rock deformation patterns in an underground mine setting.

- Compare the accuracy of static and mobile LiDAR for deformation detection.
- Assess the efficiency of mobile and static LiDAR systems in real-world applications.

### 3.3 Study site

The study was conducted at the Wits Mine Tunnel, a controlled underground mining environment at the University of the Witwatersrand's west campus (figure 10). The mock-up mine with ultramodern mining technology is at the building's basement, the roof of the building is symbolic of the upper ground surface, the stairway simulates the shaft, a 67m long shotcrete lined tunnel with a crosscut breakaway to the mine stope, lamp room and rescue chamber are constituents of the "mine".




Figure 10: Chamber of Mines building. (a) The mock “underground mine” tunnel at the lower ground section of the building. (b) A weather station situated on the roof of the main building signifies the surface of the mock underground mine.

The tunnel is accoutred with monitoring sensors that detect and record important parameters such as temperature, toxic gases, humidity, rock movements, etc (Figure 11). Among the many sensors, the tunnel has pre-existing survey coordinates and a real-time monitoring system, making it an ideal location for controlled LiDAR studies.



Figure 11: Image of the tunnel displaying rock formations, artificial lighting, ventilation pipe and blasting system.

### 3.4 Environmental Controls

To ensure the reliability and accuracy of the data sets, external factors such as lighting conditions, environmental factors (humidity, dust and temperature) and operator variability were controlled to minimise biases, especially for the mobile BLK2GO scanner, which is easily influenced by environmental conditions.

Although LiDAR technology does not depend on ambient lighting, the scans were nonetheless conducted under consistent artificial lighting (Figure 11) to ensure uniform conditions throughout the data acquisition stage. The environmental factors were controlled by scheduling the scanning for a day with stable atmospheric conditions, and the equipment was cleaned and calibrated prior to the scanning to remove dust accumulations on the sensors. Because the mobile LiDAR scanner relies on the operator's movement, which can introduce trajectory inconsistencies, affecting SLAM accuracy; a standardised closed-loop scanning trajectory was followed, and the walking pace was slow and steady to avoid drift errors.

### 3.5 Instrumentation

A combination of hardware and software was utilised to conduct the research. The following materials were used:

#### 3.5.1 LiDAR Scanners

The underground mock mine tunnel was scanned using mobile and static terrestrial LiDAR scanners at a section towards the face, where deformation is most likely to occur. The survey's primary objective was to detect geometric changes on the tunnel's surface. The Leica RTC 360 static scanner and Leica BLK2GO mobile handheld scanners were selected due to their performance against industry standards, positioning them as preferable to other LiDAR models. Previous geospatial studies have validated the scanners' precision in controlled (Kersten & Lindstaedt, 2022) and field (Grahl, 2023; Cascante *et al.*, 2020) environments, confirming their suitability for deformation monitoring. This has positioned them as suitable choices for geometric monitoring among other LiDAR models (Del Duca & Machado, 2023).

**Static LiDAR – Leica RTC360**

The Leica Geosystems RTC360 static terrestrial laser scanner (TLS) was employed.



Figure 12: The static tripod mounted terrestrial laser scanner used was the RTC 360

This LiDAR scanner has an accuracy of ≤ 2mm and a temporal resolution of ~2min per scan, capturing at least three different 360° scans from multiple locations to enhance

spatial resolution and completeness. The RTC360 TLS was mounted on a tripod (Figure 12) to provide stable, high-resolution scans. Its design makes it highly portable and efficient, as it is lightweight, does not require levelling, and records 360° spherical HDR photos in a short time, resulting in a highly detailed, colorised point cloud (Laka et al., 2019). Each area of interest within the tunnel was scanned at least three times to ensure accuracy and reliability.

The Leica RTC360 (Figure 16) features a 130-meter registry range and captures 2 million points per second, achieving a high spatial resolution of 3 mm at 10 meters. One of its key advantages is its Visual Inertial System (VIS) technology, which enables automatic registration of device displacement without the need for external targets. This feature allows seamless integration of partial point clouds, ensuring each scan is correctly aligned with subsequent ones, significantly improving the efficiency of data acquisition (Leica, 2022). Additionally, the RTC360 can capture a 360-degree point cloud image in under two minutes, making it one of the fastest and most efficient scanning solutions available (Cascante *et al.*, 2020). These state-of-the-art technical characteristics made it ideal for capturing detailed, high-resolution data for this study.

**Mobile LiDAR – Leica BLK2GO**

The second scanner used in this study was the Leica BLK2GO, an ergonomic, handheld mobile LiDAR scanner (Figure 13). This device captures point clouds in real-time while simultaneously acquiring moving images, utilising Simultaneous Localisation and Mapping (SLAM) technology to track its movement through space. The BLK2GO is equipped with dual-axis LiDAR sensors, a 4.3-megapixel camera with 360-degree panoramic viewing, a 12-megapixel high-resolution camera for capturing detailed imagery, and an inertial measurement unit (IMU) for self-navigation and motion tracking. It captures 420,000 points per second within a 0–25-meter range (Del Duca & Machado, 2023).



Figure 13: Leica BLK2GO Handheld Imaging Laser Scanner (Leica Geosystems, 2022).

To achieve maximum accuracy, the system employs Grand-SLAM technology, delivering 6–15 mm relative precision and 20 mm absolute positioning accuracy (Cascante *et al.*, 2020).

During the data acquisition process, the captured point clouds were continuously evaluated and optimised to ensure seamless integration of scans from different positions. The Leica Cyclone FIELD 360 application, installed on a mobile tablet, facilitated real-time pre-processing on-site. The scanner and tablet were linked via a Wi-Fi network, enabling automatic wireless data transfer to the tablet in real-time. Once scanning was completed in the field, the data was transferred to a desktop workstation for further processing, refinement, and analysis.

### 3.5.2 Control Survey Equipment

As a fundamental requirement for laser scanning, the georeferencing method employed was the conventional approach, as explained in Section 2.10. This method was selected for its high precision and flexibility, particularly because it does not require height measurements or levelling of the laser scanner. Additionally, it does not require the laser scanner to be positioned directly beneath pre-established control points, making it advantageous for capturing the geometric details of un-surveyed and restrictive stope areas without compromising accuracy (Laka et al., 2019).

#### Leica TS03 Total Station

To establish a reliable control network, the Leica TS03 Total Station (Figure 14) was used to provide high-precision coordinate referencing. This instrument is known for its angular accuracy of 1” (one arc-second) and distance measurement accuracy of ±1 mm + 1.5

ppm, making it ideal for underground deformation monitoring where precise spatial referencing is critical (Leica Geosystems, 2019).



Figure 14: Total station and target set up to determine the coordinates and height of the three tie points.

### 3.6 Data processing

To ensure efficient and accurate point cloud processing, it is important to use the software associated with the scanner to minimise error components (Kersten & Lindstaedt, 2022), the following software tools described in Table 3 were used:

Table 3: Software used to capture and process the raw point data.

| Work phase | Software | Import format | Export format |
|---|---|---|---|
| UTM referencing | Infinity | ASCII | – |
| Scanning and pre-processing | Field 360 | Direct Wi-Fi connection | Direct export to Leica Cyclone 360 |
| Processing | Cyclone register 360 Cloud Compare | LGS, PXT, PTS, E57 | Various formats, including point clouds and geometries |
| Accuracy Assessment | Cyclone Register 360 | – | Various |
| Results visualisation | TruView Cloud Compare | LGS, LAS | Various |

Once the raw data was pre-processed, an analysis was conducted using the robust open-source CloudCompare software. The following parameters were carefully selected on the CloudCompare software based on computational efficiency and accuracy. The point cloud was trimmed so that only the section close to the face was considered. Further segmentation was performed to reduce computation time and only the face, tunnel sides, and roof were analysed independently.

The point clouds with a higher point density were subsampled to match the lowest point density, and a point spacing of neighbouring points was applied at a 0.05m radius. This was considered to be the surface density output (Fryskowska-Skibniewska & Wróblewski, 2018). Normal computation was conducted using a quadratic surface fitting; this method is appropriate for detecting curved surfaces (Lague *et al.*, 2013) such as the shapes of our deformation simulations at a 0.5m radius to ensure a smooth local surface model. The normals were orientated using the minimum Spanning Tree function with 10 neighbours, to balance computational efficiency. The surfaces were then created using the Poison surface reconstruction algorithms at an octree depth of 10, for a high resolution. The change detection deviation threshold was set to 0.05m, which falls below the deformation classification for underground mining tunnels deemed relatively “safe” (Hadjigeorgiou & Potvin, 2023). This was done to identify significant deformations.

## 3.7 Data Collection

### 3.7.1 Identifying and Mapping Rock Deformation (Objective A)

Since real rock deformation is unpredictable, the study used solid materials with known dimensions to simulate deformation scenarios. These simulations were based on geological principles (Kentucky Geological Survey, 2019) detailed in Section 2.5:

a) **Boulder Formation Simulation:**

Large artificial boulders (Figure 15) were placed at critical tunnel locations to test change detection, modelling weathered rock masses prone to instability and deformation.

Constructed using Styrofoam and plastic to resemble real geological structures (Dan et al., 2016).



Figure 15: Irregular boulder structure randomly placed as an unstable cornerstone at the face of the tunnel to simulate the concept described by Dan et al., (2016).

b) **Kettlebottom Roof Failure Simulation:**

Plastic bags filled with paper were suspended (Figure 16) to mimic sagging rock masses, as described by Deng et al. (2019). This approach ensured minimal shape distortion and realistic displacement representation.



Figure 16: Deformation simulation of a semi-circular rock mass, sagging from an underground mine roof

c) **Cavern and Bulging Sidewall Deformation Simulation:**

Simulated rock bursts resulting from stress release in tunnel walls (Judeel, 2003).

Bulges of random shapes (Figure 17) were placed at random along the tunnel walls, roof, and face.

### 3.8 Maximum distance computation as displacement

The thickness or maximum displacement from the surface of the deformation objects was measured once they were positioned in their relative spaces. These distance measurements were repeated ten times or more in some instances, around the object and the maximum distance from the surface was computed as the displacement value.




Figure 17: Underground tunnel displaying pre-and post-deformation simulation for rock burst scenario on the tunnel's rock surface

### 3.9 Evaluating the Accuracy of Static and Mobile LiDAR (Objective B)

#### 3.9.1 Total Station Georeferencing:

Three tie points were established using the Leica TS03 Total Station to serve as fixed reference locations. The first step involved creating a target network ( ST1, ST2, ST3) by strategically placing three specially designed targets in locations visible along the LiDAR scanners' line of sight (Figure 18). Since 3D geodetic global system information was not inherently available for the selected target points, a total station system was introduced to transfer both horizontal and vertical control network data onto these targets (Leica, 2022). This process entailed:

1. Determining the total station's global horizontal coordinates using pre-existing control points.
2. Levelling the system by transferring height differences from vertical control points to the total station.

3. Measuring and establishing the tie-points' 3D coordinates using the total station's position.




Figure 18: Target network of three tie points (ST1, ST2, ST3) selected for the registration of the laser data

Following these steps, the terrestrial laser scan georeferencing was determined through a rigid body transformation, aligning different scans via the transformation matrix (*T*), which includes both rotation (*R*) and translation (*t*), as expressed in Equation (3) (Kim & Seo, 2020):

$$p' = R.p + t \qquad (3)$$

$p$ = original point coordinates (from the moving point cloud)

$p'$ = transformed point coordinates (aligned with the reference point cloud)

$R$ = 3x3 rotation matrix

$t$ = 3x1 translation vector

The integration of the Leica TS03 Total Station into the static and mobile LiDAR scanners facilitated the generation of a precise and well-referenced point cloud, producing accurate deformation monitoring in the underground mine.

### 3.9.2 LiDAR Point Cloud Registration:

The alignment or matching of scans into a single coordinate system was first done in the field by matching similar targets captured in scans as reference and on the Cyclone Register360 using the automated Iterative Closest Point algorithm (4), widely applied in software programs, capable of minimising scan alignment errors between corresponding point clouds (Procházková & Martišek, 2018) by solving:

$$E(R,t) = \frac{1}{N}\sum_{i=1}^{N} \| R.p_i + t - q_i \|^2 \qquad (4)$$

- $E(R,t)$ = error function to be minimised
- $p_i$= points from the moving point cloud
- $q_i$ = corresponding points in the reference point cloud
- $N$ = number of points
- $R$ = rotation matrix
- $t$ = translation vector

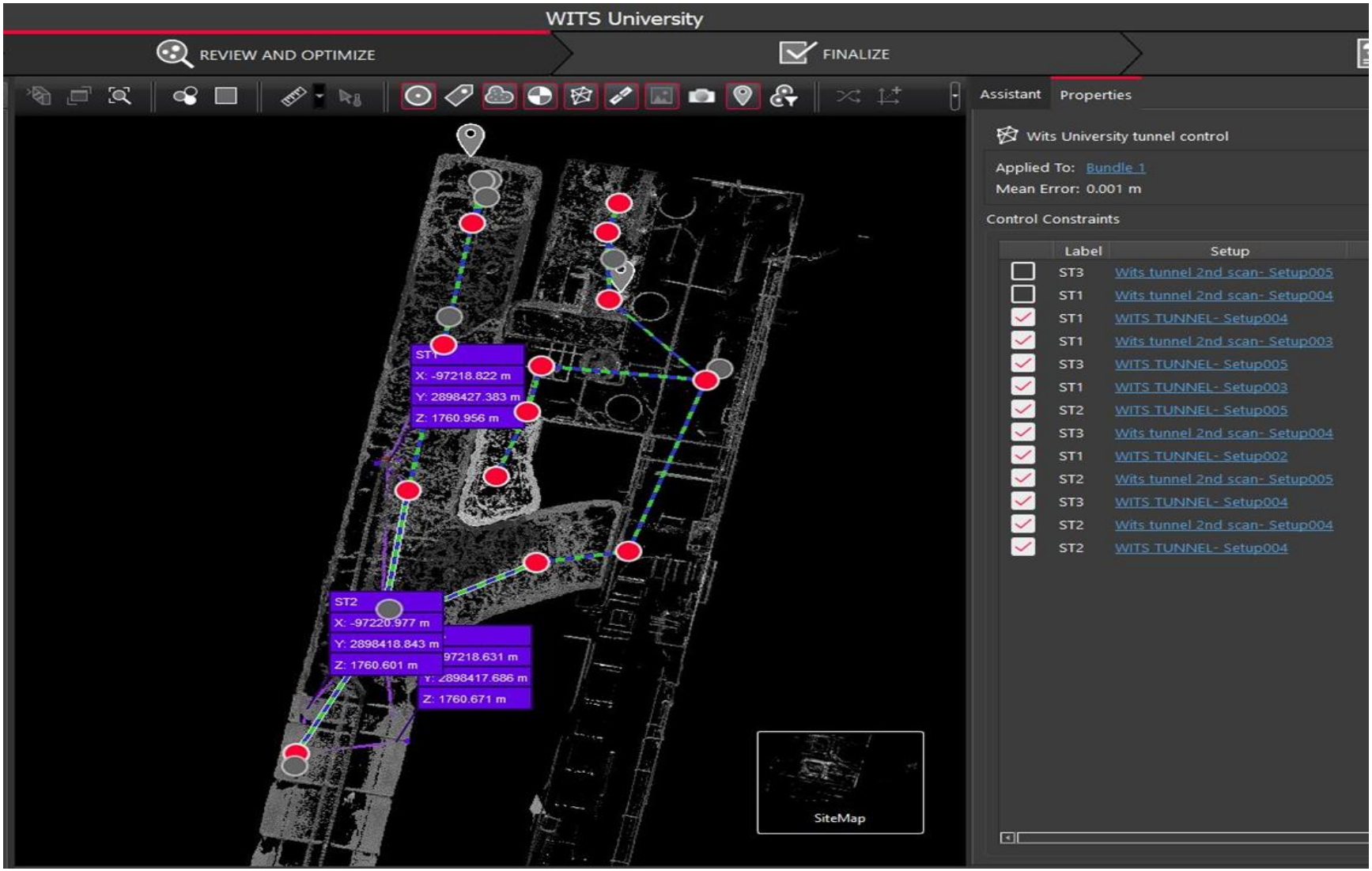



Figure 19: Registration of scans to a unified coordinate system, showing a closed-loop trajectory of mobile laser scanning with total station positions and computed X, Y, and Z values.

Fixed survey co-ordinates within the scan environment were used as our control points, and they were kept constant throughout all scans to avoid target resetting uncertainties (Silvia & Olsen, 2012). The open-source Cloud Compare software was then used to convert the point cloud data into a spatially referenced surface model.

### 3.10 Metrics for accuracy and reliability assessment:

For the assessment of the accuracy and reliability of LiDAR-derived deformation measurements, three key statistical metrics were selected: Root Mean Square Error (RMSE), Mean Absolute Error (MAE), and the Coefficient of Determination ($R^2$). These metrics were chosen due to their widespread application in geospatial accuracy assessment, particularly in LiDAR-based deformation studies (Singh *et al.*, 2023). Each metric provides unique insights into measurement discrepancies and contributes to a comprehensive evaluation of LiDAR accuracy.

#### 3.10.1 Root Mean Square Error (RMSE)

In geospatial analysis, RMSE is a widely utilised statistic for quantifying the deviation of observed values from reference data (Kouzehgar & Eslamian, 2023). It provides a measure of precision by penalising larger errors more than smaller ones, making it particularly useful for evaluating systematic and random errors in LiDAR point cloud datasets (Kim & Seo, 2020). RMSE is computed as follows:

$$RMSE = \sqrt{\frac{1}{n}\sum_{i=1}^{n}(X_i - X_{ref,i})^2} \quad (5)$$

where:

- $X_i$ = LiDAR-measured values,
- $X_{ref,i}$= reference field measurements,
- $n$ = 7 (total number of observations).

A lower RMSE indicates better alignment between LiDAR-derived and ground truth measurements (Fuad *et al.*, 2018). Since deformation studies require high precision, RMSE was selected to identify subtle deviations in LiDAR-derived surface changes.

### 3.10.2 Mean Absolute Error (MAE)

MAE was included as a complementary metric to RMSE because it provides a more intuitive interpretation of error magnitude. Unlike RMSE, which squares errors and amplifies larger deviations, MAE treats all errors equally, making it useful for assessing the average measurement discrepancy (Gao & Wu, 2021). It is calculated as:

$$MAE = \frac{1}{n}\sum_{i=1}^{n}\left|X_i - X_{ref,i}\right| \quad (6)$$

MAE is often preferred when analysing datasets with outliers, as it does not disproportionately emphasise extreme values (Zhou *et al.*, 2024). Since deformation monitoring involves complex surfaces with potential variations in error distribution, MAE was selected to complement RMSE and provide a more balanced error assessment.

### 3.10.3 Coefficient of Determination ($R^2$)

The coefficient of determination ($R^2$) was chosen to assess the correlation between LiDAR-derived measurements and ground truth data. It quantifies how well the LiDAR measurements explain variations in actual deformation, making it an essential metric in geospatial studies (Chen *et al.*, 2019) . The formula for $R^2$is:

$$R^2 = 1 - \frac{\sum(X_{ref,i} - X_i)^2}{\sum(X_{ref,i} - \bar{X}_{ref,i})^2} \quad (7)$$

where $\bar{X}_{ref}$ represents the mean of the reference values.

An $R^2$ value close to 1 indicates a strong correlation, confirming the reliability of LiDAR for deformation mapping (Onyutha, 2020). This metric was particularly important in this study to evaluate the consistency of LiDAR measurements across different deformation features.

### 3.10.4 Paired t-Test

The paired t-test was conducted to assess if the mean difference between the mobile and static LiDAR measurements was statistically significant. This test tool was chosen because both LiDAR systems are related, therefore directly comparable. The paired t-test compares the average difference between the two sets of measurements (Ajayi & Palmer, 2020) collected at seven common features (face bulge; roof boulders 1 and 2;

left-wall bulge and boulder; right-wall bulge and caving), giving a sample size n = 7 from the formula:

$$t = \frac{\bar{d}}{s_{d/\sqrt{n}}} \quad (8)$$

Where:

$\bar{d}$ = average difference between mobile and static LiDAR measurements

$s_d$ = standard deviation of differences

$n$ = number of measured pairs

The final t-test value (t-score) is compared to the critical t-value with *df*= $n$ – 1, from the t-distribution table at a 95% (p-value of 0.05) confidence interval (Ajayi & Palmer, 2020). A p-value helps determine whether there is a significant difference between the 2 LiDAR systems relative to the variation in the data. A higher t-value suggests minimal difference, while p ≤ 0.05 suggests statistical significance, and a p-value > 0.05 means both LiDAR systems produced comparable results.

**M3C2 Algorithm for Deformation Analysis**.

The pre-deformation (T1) and post-deformation (T2) point clouds were processed using M3C2 to compute surface displacement. The algorithm was applied to different deformation zones, including tunnel walls and the roof. Displacement maps were generated to visualise the magnitude and distribution of deformation within the underground environment. The confidence intervals associated with M3C2 measurements were analysed to assess the reliability of the detected changes.

The Multiscale Model-to-Model Cloud Comparison (M3C2) algorithm was employed in this study to quantify and analyse deformation within the underground mining environment. M3C2 is specifically designed for direct 3D comparison of point clouds, making it highly effective for detecting surface changes over time. Unlike traditional point cloud comparison methods, M3C2 operates by computing distances along the normal direction of the surface, allowing for accurate deformation assessment while incorporating uncertainty estimation (Lague *et al.*, 2013)

M3C2 calculates point-wise distances between pre- and post-deformation scans (T1 and T2) along a local normal vector derived from the surface geometry. This approach minimises errors related to scan misalignment and varying point cloud densities. The displacement at each point is determined using:

$$d_{M3C2} = \frac{1}{n}\sum_{i=1}^{n}(p_i, T2 - p_i, T1) \cdot N_i \quad (9)$$

Where:

- $d_{M3C2}$ = computed displacement along the normal vector,
- $p_i, T1$ and $p_i, T2$ = corresponding points from pre- and post-deformation scans,
- $N_i$ = surface normal vector at $p_i, T1$
- $n$ = number of neighbouring points considered for the calculation.

In this study, the *n* value in the M3C2 displacement formula (Equation 9) represents the number of neighbouring points used to estimate the local surface normal and compute distances along it (Lague et al., 2013). Instead of assigning a fixed *n* value across all segments, the parameter was determined algorithmically in CloudCompare using the *"subsample cloud #1"* option. This option automatically defines the neighbourhood size relative to the density of the subsampled reference cloud, ensuring consistency across different geometrical segments (face, roof, and side walls). Although the exact numerical *n* values were not exported, the approach ensures that neighbourhood sizes were proportionally adapted to local point densities, thus balancing accuracy and noise reduction (Girardeau-Montaut, 2015).

# Chapter 4

## 4 Results

### 4.1 Introduction

This chapter presents the results of the methodology described in Chapter 3. Firstly, it focuses on the post-processing and analysis of data collected during the study. It begins with a pre-analysis of data quality to ensure reliability. Mesh-to-mesh deformation mapping and visualisation techniques are detailed, and deformation measurements obtained from simulated formations are compared using field methods, static, and mobile LiDAR platforms. Statistical analyses, including Root Mean Square Error (RMSE), Mean Absolute Error (MAE), and the coefficient of determination ($R^2$), are applied to assess accuracy. The operational efficiency of static and mobile LiDAR systems in detecting rock deformation is evaluated. Finally, the chapter concludes by discussing the results and the research limitations.

### 4.2 Post-Processing Comparison of Static and Mobile LiDAR

The point clouds generated by the mobile and static LiDAR scanners were registered and subsequently segmented to focus on the region near the tunnel face (Figure 20). This segmentation reduced computational complexity, enabling more efficient processing and targeted analysis of key areas.

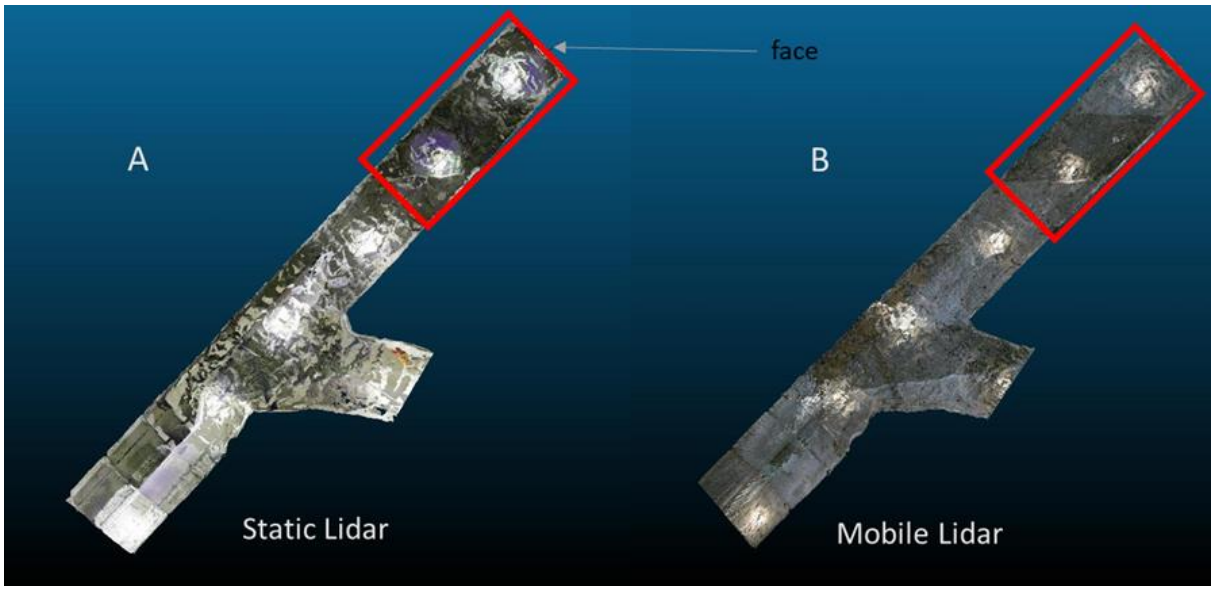



Figure 20: Static and mobile LiDAR point cloud model of the tunnel, with the red block showing the segmented section along the tunnel where the analysis occurred.

It additionally facilitated clearer visualisation and a more direct comparison of the computed results.

### 4.2.1 Point Cloud Characteristics

The post-processed results (Figure 21) present a comparative analysis of point cloud data acquired from static and mobile LiDAR systems, emphasising variations in resolution, point density, the spatial distribution of points, and overall scan fidelity for both pre-and post-deformation conditions.




Figure 21: Post-processing contrast of segmented, pre- and-post deformation point-cloud scans from both static and mobile LiDAR platforms

The static LiDAR point clouds present evenly distributed and densely packed points due to the scanner's fixed position, which enhances resolution and captures the detail of small features. Point density remains relatively consistent across the tunnel's left and right walls, the face, and roof. In contrast, mobile LiDAR scans present streaky, noisy, and irregularly distributed points. This result is influenced by the scanning mechanism, movement variations, and platform movement speed because mobile LiDAR collects data in sequential strips along a trajectory. The overlaps, also known as misalignment of consecutive strips, cause streaky patterns; these are more pronounced when scanning

angles are inconsistent because of hand motion instability. The variations in point density for left and right walls pre- and post-deformation for mobile LiDAR are caused by variations in speed. It is also observed that static LiDAR is prone to occlusion due to its stationary nature, which limits its perspective, creating shadows and gaps where the scanner cannot 'see,' Figure 22 illustrates this whilst highlighting potential differences in resolution and point density.

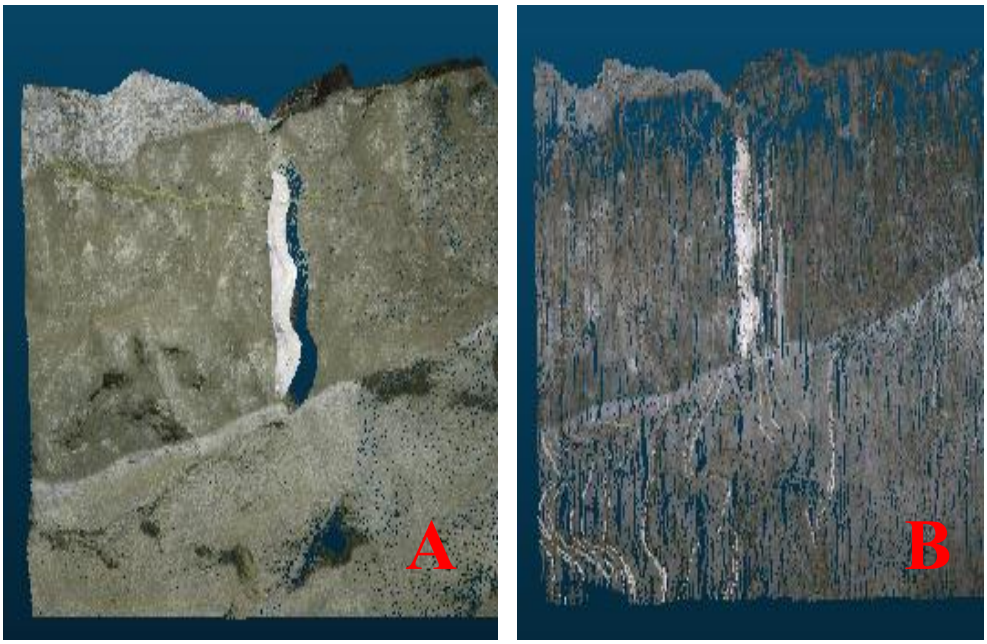



Figure 22: Comparison of occlusion effects in static and mobile LiDAR scans. A (static LiDAR), occlusion is visible behind the object leaving gaps due to restricted line of sight. B (mobile LiDAR), reduced occlusion because of moving scanner capturing multiple perspectives

### 4.2.2 Point cloud registration

To ensure accuracy in deformation analysis, fine registration was performed on the segmented pre- and post-deformation scans. Surface errors (Table 4) quantify the deviations in registered surfaces, providing insights into data quality.

Table 4: Surface errors for the different segments of the tunnel. Surface errors were generated after fine-registering the pre- and post-deformation scans with one another.

| **Surface** | **Error** |
|---|---|
| Right wall mobile | 0.0197979 |
| Right wall static | 0.0101897 |
| Left wall static | 0.020598 |
| Left wall mobile | 0.0205449 |

| | |
|---|---|
| Tunnel Face static | 0.0118265 |
| Tunnel Face mobile | 0.0147769 |
| Roof mobile | 0.00941602 |
| Roof static | 0.0133027 |

From these results, it is observed that static scans of the right wall produced lower surface error compared to the mobile scanner. The left wall yielded similar errors between the mobile and static scanners. The tunnel face provided slightly better accuracy than the static scanner. The static scanner produced lower errors for the vertical surfaces (walls and face) because of its stable position and denser data acquisition. However, for the horizontal roof, the mobile scanner outperformed the static scanner. This result could be attributed to differences in sensor angles or poor capture strategy. Overall, the low registration errors across all the scans indicate reliable alignment, subsequently allowing for accurate surface reconstruction (Figure 23) and deformation analysis.

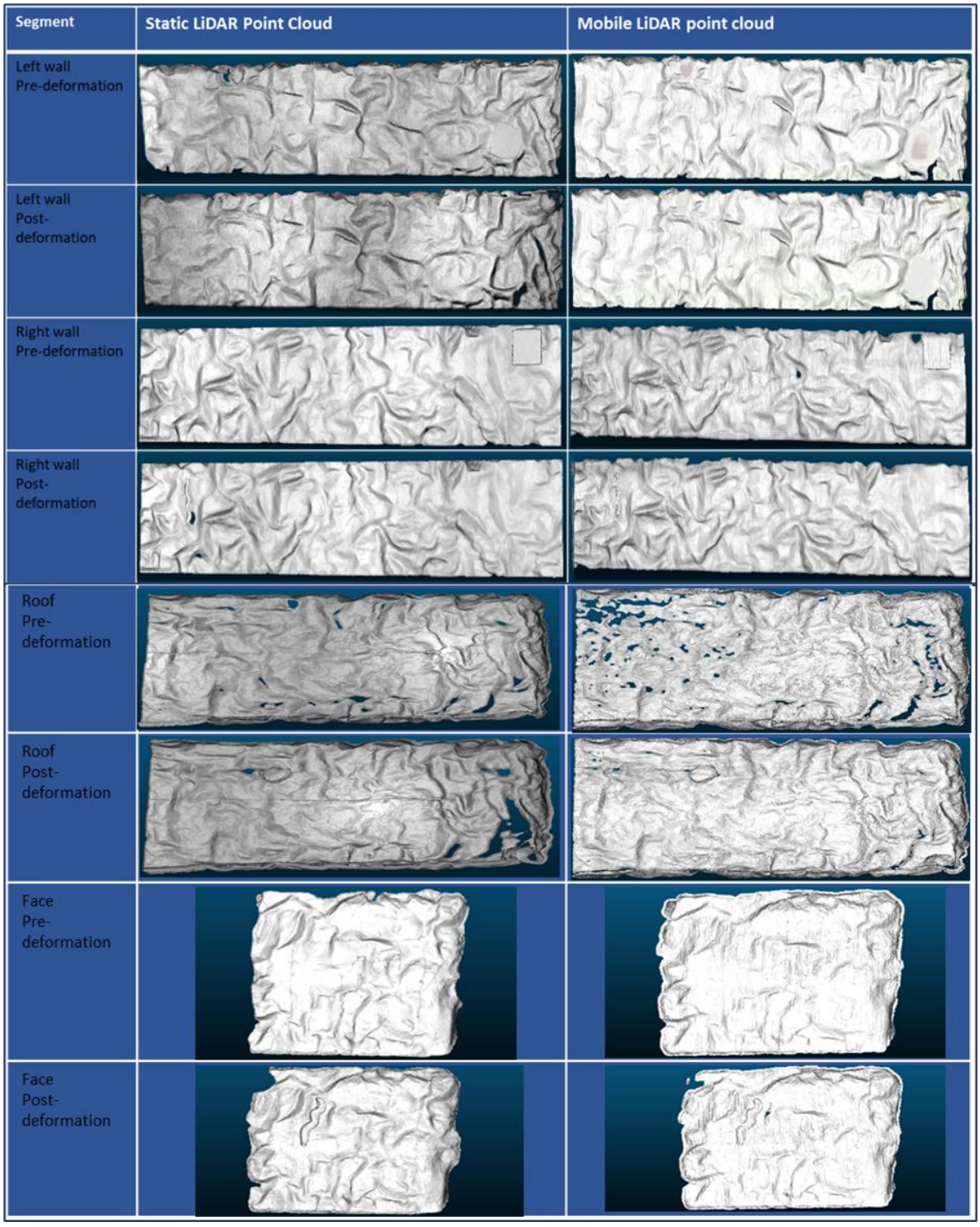



Figure 23: Reconstructed 3D surface models for pre- and post-deformation segments of the tunnel.

### 4.3 Deformation Mapping and Visualisation

Deformation measurements were derived by computing distances between pre- and post-deformation surfaces using CloudCompare's Multiscale Model-to-Model Cloud Comparison (M3C2) algorithm.

The analysis presented a series of visualisations using a colour-coded scheme, where warm colours (red and yellow) indicate outward deformation or material addition, and cool colours (blue and green) signify inward deformation or material loss, as depicted in Figure 24. A neutral colour (white) represents regions with no significant change. This section presents the deformation results, highlighting the spatial distribution and magnitude of the observed changes in the tunnel, segmented as the left and right walls, the face, and the roof.

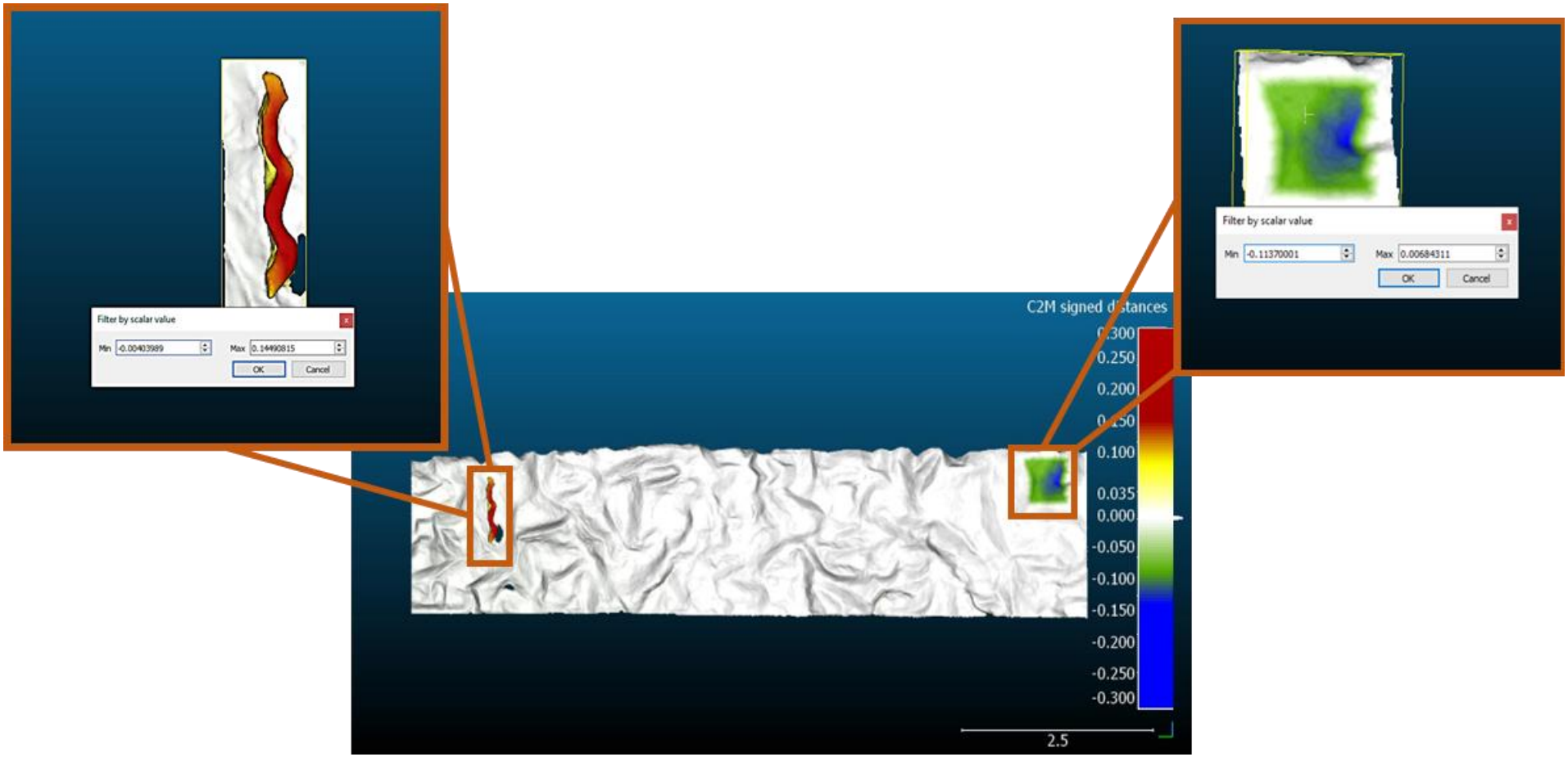



Figure 24: Computation of maximum/minimum deformation distance from detected areas of deformation using statistical computation function. Deformation areas are colour-coded, with warm colours indicating outward deformation and cool colours showing inward deformation.

**Spatial Distribution of Deformation**

For the left-wall, significant outward deformation is observed in localised regions, highlighted by red zones, particularly near the top-left and bottom-right sections of the mobile and static scans of Figure 25. These indicate bulging material. In contrast, the right wall shows a prominent vertical deformation zone in static and mobile scans, with red bands suggesting significant outward deformation. A localised blue and green area on the far top right of the right wall indicates an inward deformation or material loss. The roof section exhibits distinct deformation patterns, showing a pronounced red zone in the lower centre of the roof and the bottom left corner of the scans, suggesting material bulging.

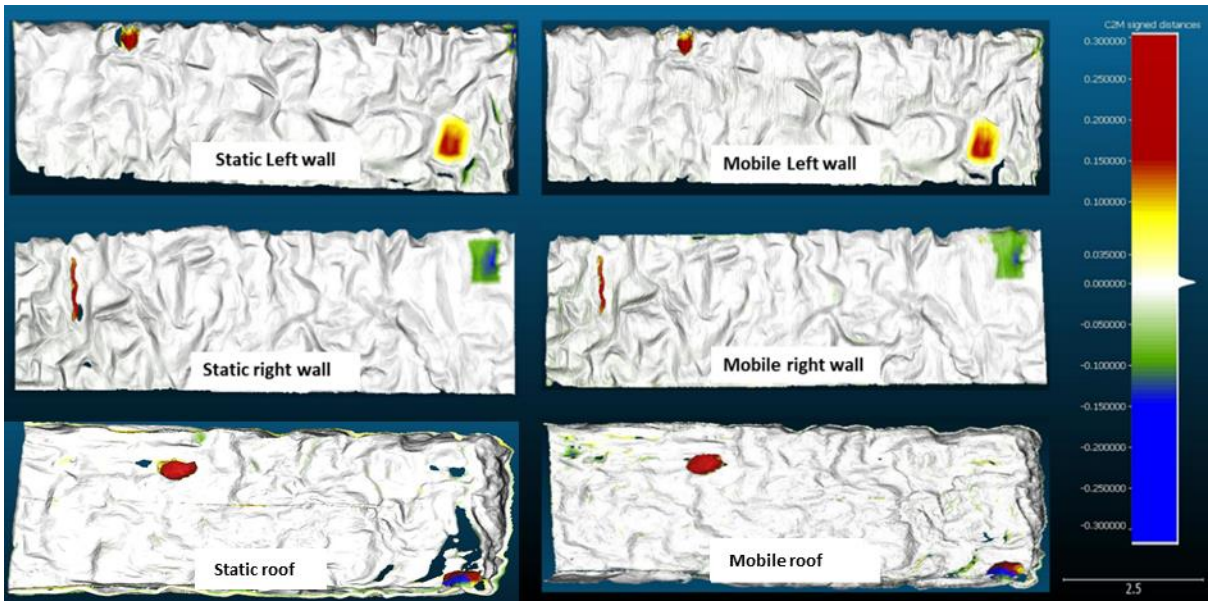



Figure 25: Contrast of static and mobile LiDAR segments, presenting localised deformations. Warm colours (red and yellow) indicate outward deformation or material addition, and cool colours (blue and green) signify inward deformation or material loss.

Minimal deformation is observed elsewhere on the walls, as indicated by the predominantly white areas. However, these regions of minimal deformation result from errors caused by gaps in the point cloud data due to poor data quality. Such gaps could not be interpolated during the meshing process, leading to false distance changes or discrepancies in areas that otherwise show no significant deformation.

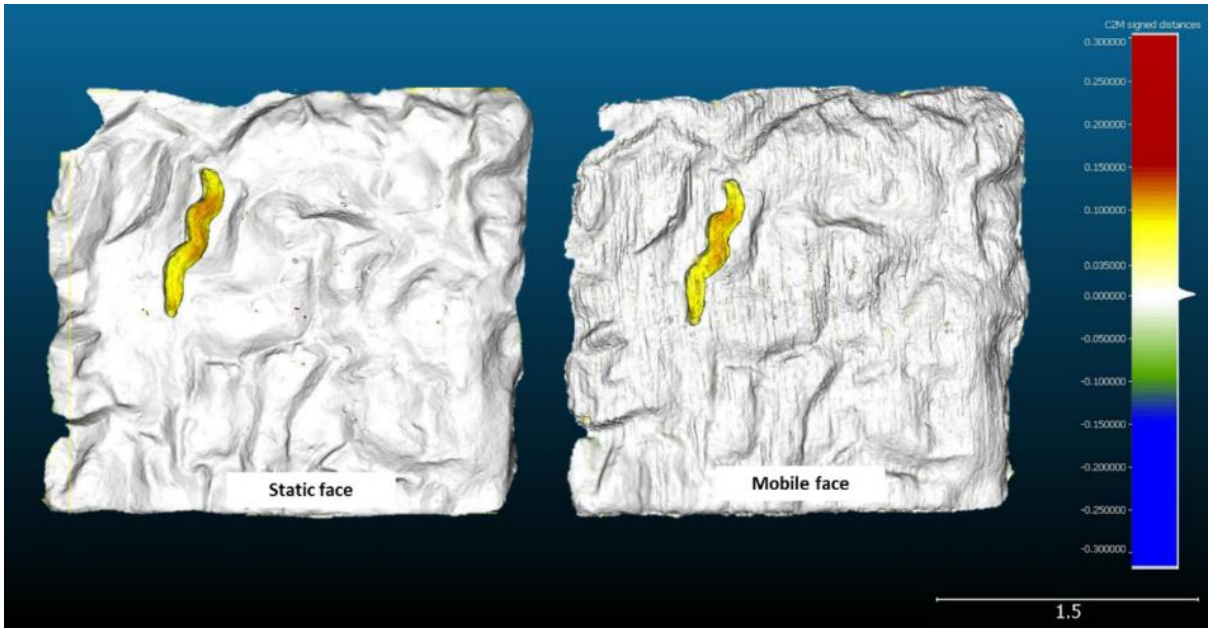



Figure 26: Contrast of static and mobile LiDAR face segments, presenting localised deformation.

The deformation analysis of the tunnel face (Figure 26), as shown in the static and mobile LiDAR scans, highlights a localised deformation zone. Both scans display a consistent pattern of deformation, represented by the yellow region in the centre of the tunnel face, corresponding to positive displacement or outward deformation. This suggests bulging in this specific area.

The consistency between the static and mobile scans in the deformation zone signifies reliability in the data acquisition and analysis process. The surrounding areas mainly show a neutral or white colour, indicating no deformation. Minor discrepancies or noise around the edges of the deformation zone are attributed to the data gaps or interpolation errors during the meshing process, particularly in regions with poor point density. These errors result in false distance changes, emphasising the importance of high-quality data acquisition for precise deformation analysis.

The overall visualisation of these results indicates distinct deformation patterns across the tunnel, with notable changes localised to specific regions. Although the mobile and static LiDAR platforms yielded similar results, inaccuracies due to data gaps illuminate and iterate the importance of ensuring high data quality during scanning and meshing.

### 4.4 Deformation Measurement Accuracy

Deformation values from static and mobile LiDAR were compared against field measurements (Table 8). Both LiDAR systems closely matched field-measured deformations, with discrepancies within a few millimetres.

Table 5: Comparison of deformation measurements for the simulated formations was measured using field methods and static and mobile LiDAR platform measurements.

| **Feature** | **Field measurement (m)** | **Mobile LiDAR measurement (m)** | **Static LiDAR measurement (m)** |
|---|---|---|---|
| Face | | | |
| Linear bulge | 0.10 | 0.0979 | 0.0998 |
| Roof | | | |
| Boulder 1 | 0.270 | 0.247 | 0.254 |
| Boulder 2 | 0.220 | 0.211 | 0.214 |
| Left wall | | | |
| bulging wall | 0.155 | 0.140 | 0.137 |
| Boulder | 0.220 | 0.187 | 0.185 |
| Right wall | | | |
| Linear bulge | 0.160 | 0.140 | 0.144 |
| Caving wall | 0.100 | 0.091 | 0.113 |

*Face*

The linear bulge deformation values from the mobile and static LiDAR closely align with field measurements, indicating a high accuracy for both scanning platforms.

*Roof*

The deformation for Boulders 1 and 2 show slightly higher discrepancies, especially for Boulder 1, where the mobile LiDAR result underestimates the field measurement by 0.023m. These differences could arise from the irregular shape features, where interpolation errors during meshing might have affected the accuracy.

*Left wall*

The bulging wall and boulder's mobile and static LiDAR measurements show underestimations compared to the field measurements and differ minimally from one

another. This shows a consistent trend of slight underestimation in wall features, probably because of the data gaps and complexity of capturing vertical surfaces accurately.

*Right wall*

The linear bulge measurements are underestimated, while the caving wall feature presents a slightly larger discrepancy. Here, the static LiDAR overestimates the field measurements by 0.013, likely due to localised interpolation or noise during the meshing process. Figure 27 compares the measurements discussed in this section.

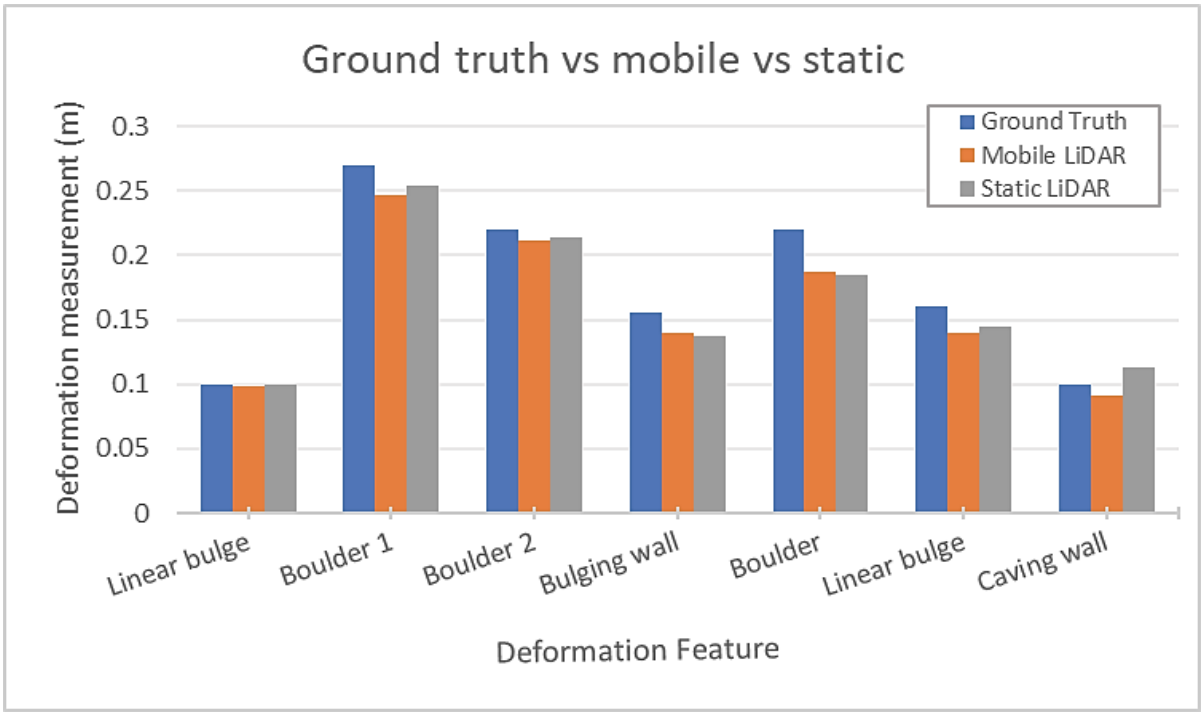



Figure 27: Comparison of deformation measurements computed from the LiDARs tested against the ground truth measurements.

### 4.4.1 Statistical Analysis

#### 4.4.1.1 Root mean square error (RMSE)

The overall RMSE computed in Table 9 shows that mobile and static LiDAR measurements provide highly accurate deformation mapping. Static LiDAR measurements exhibit better accuracy, as noted by a lower RMSE of 0.0180 compared to the Mobile LiDAR's relatively higher RMSE value of 0.0186. This tells us that static LiDAR may be preferred for precise deformation monitoring, particularly in scenarios where even minor discrepancies could be critical.

Table 6: RMSE for mobile and static LiDAR calculated from ground field measurements vs LiDAR data.

| Feature | Field Measurement (m) | Mobile LiDAR Measurement (m) | Static LiDAR Measurement (m) | RMSE (Mobile LiDAR) | RMSE (Static LiDAR) |
|---|---|---|---|---|---|
| Linear bulge | 0.100 | 0.0979 | 0.0998 | 0.0021 | 0.0002 |
| Boulder 1 | 0.270 | 0.247 | 0.254 | 0.0230 | 0.0160 |
| Boulder 2 | 0.220 | 0.211 | 0.214 | 0.0090 | 0.0060 |
| Bulging wall | 0.155 | 0.140 | 0.137 | 0.0150 | 0.0180 |
| Boulder | 0.220 | 0.187 | 0.185 | 0.0330 | 0.0350 |
| Linear bulge | 0.160 | 0.140 | 0.144 | 0.0200 | 0.0160 |
| Caving wall | 0.100 | 0.091 | 0.113 | 0.0090 | 0.0130 |
| Overall RMSE | | | | **0.0186** | **0.0180** |

#### 4.4.1.2 Mean absolute error (MAE)

Based on the tabulated results (Table 9), the static LiDAR shows slightly lower overall MAE compared to the Mobile LiDAR, indicating slightly better agreement with ground truth field measurements. The differences between the two platforms are minimal, suggesting that both platforms provide high accuracy for deformation mapping, but the static LiDAR has a higher accuracy in this dataset.

Table 7: MAE for mobile and static LiDAR calculated from ground field measurements vs LiDAR data.

| Feature | Field Measurement (m) | Mobile LiDAR (m) | Static LiDAR (m) | MAE (Mobile LiDAR) | MAE (Static LiDAR) |
|---|---|---|---|---|---|
| Linear Bulge (Face) | 0.1 | 0.0979 | 0.0998 | 0.0021 | 0.0002 |
| Boulder 1 (Roof) | 0.27 | 0.247 | 0.254 | 0.023 | 0.016 |
| Boulder 2 (Roof) | 0.22 | 0.211 | 0.214 | 0.009 | 0.006 |
| Bulging Wall (Left Wall) | 0.155 | 0.14 | 0.137 | 0.015 | 0.018 |
| Boulder (Left Wall) | 0.22 | 0.187 | 0.185 | 0.033 | 0.035 |
| Linear Bulge (Right Wall) | 0.16 | 0.14 | 0.144 | 0.02 | 0.016 |

| | | | | | |
|---|---|---|---|---|---|
| Caving Wall (Right Wall) | 0.1 | 0.091 | 0.113 | 0.009 | 0.013 |
| Average MAE (m) | | | | **0.01587** | **0.01489** |

#### 4.4.1.3 Coefficient of determination ($R^2$)

The scatter plots (Figure 28) illustrate the relationship between deformation measurements obtained from a) mobile LiDAR, b) static LiDAR and ground truth data field measurements. The x-axes represent the ground truth measurements (m), which is the reference standard, while the y-axes represent the corresponding measurements recorded by the mobile and static LiDARs (m).

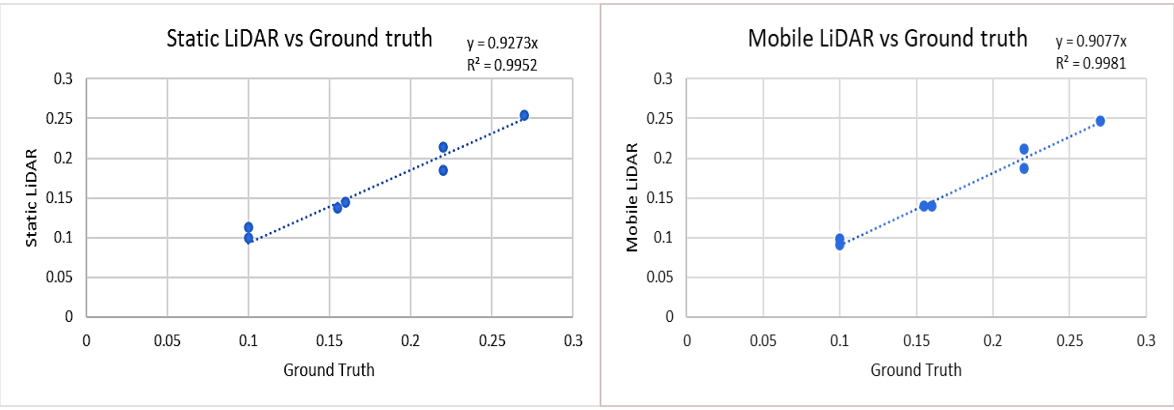



Figure 28: $R^2$ relationship between deformation measurements obtained from a) mobile LiDAR, b) static LiDAR and ground truth data field measurements

A linear regression line was fitted to the data, yielding the equation *y*=0.9077*x* with a coefficient of determination ($R^2$) value of 0.9981 for mobile LiDAR data, and *y*=0.9273*x* and an $R^2$ Value of 0.9952 for static LiDAR. Both platforms strongly correlate with the ground truth data as they are closer to 1. The slightly higher $R^2$ Value yielded by mobile LiDAR suggests better accuracy of mobile LiDAR for deformation mapping. However, the slope of the regression line (0.9077) suggests a slight underestimation by the mobile LiDAR compared to the ground truth values. These results imply that both LiDAR systems are dependable for mapping deformation. Mobile LiDAR may provide a marginally stronger alignment to the field measurements, making it effective for environments requiring the flexibility and mobility it offers (Singh *et al.*, 2023). Furthermore, a paired t-test was performed to determine if the differences between mobile and static LiDAR measurements are statistically significant, to which the p-value was greater than 0.188,

a value greater than the commonly used threshold of 0.05. This indicated no statistically significant difference.

From what we can gather from the statistical analysis of the deformation results, considering the root mean square error (RMSE), mean absolute error (MAE), and coefficient of determination ($R^2$), static and mobile LiDAR platforms offer accuracy and reliability. The RMSE values indicated small deviations between LiDAR measurements and field measurements, where static LiDAR demonstrated slightly lower errors compared with mobile LiDAR. The MAE analysis reinforces these findings, showing that the static LiDAR platform's measurements are slightly closer to field measurement values, which reflects a higher precision than the mobile LiDAR platform. The $R^2$ values, which measure the correlation between LiDAR and field data, demonstrated strong agreement for both the LiDAR platforms, indicating their suitability for deformation monitoring. All these metrics illuminate the robustness of mobile and static LiDAR systems but prove static LiDAR to have superior accuracy in this study.

### 4.5 Assessing the operational efficiency of static and mobile LiDAR systems in detecting rock deformation.

Operational efficiency is critical when choosing an appropriate LiDAR platform for rock deformation monitoring in underground environments. It influences the speed, quality, and reliability of data acquisition, as well as its adaptability to complex underground conditions (Rashdi *et al.*, 2024; Wang *et al.*, 2024). Having used both mobile and static LiDAR platforms and obtained deformation results, the following comparison can be tabulated, highlighting the strengths and limitations of the system in practical application.

Table 8: Overview of operational efficiency of static and mobile lidar systems.

| Criterion | Static LiDAR | Mobile LiDAR |
|---|---|---|
| **Data Acquisition Speed** | Slower due to stationary setup and needs multiple scans to cover large areas. | Faster, as the scanner can capture data while moving, allowing quick coverage of extensive areas. |

| | | |
|---|---|---|
| **Setup Time** | Requires more time to set up at each scanning station, including levelling and calibration. | Minimal setup time: ready to use as the operator moves through the environment. |
| **Accessibility** | Limited by the scanner's fixed position; some areas may remain unreachable without repositioning. | Better accessibility, as the scanner can manoeuvre through tight or complex spaces. |
| **Point Cloud Density** | Higher, as scans are conducted from fixed positions with stable proximity to the surfaces. | May have a lower density in some areas due to motion-induced variability or trajectory challenges. |
| **Proximity to Surfaces** | Fixed proximity allows for consistent and high-quality scans, especially in challenging areas. | Requires careful operator management to maintain optimal distance for consistent data quality. |
| **Mobility** | Less mobile; relies on stable platforms for operation. | Highly mobile, making it suitable for dynamic environments. |
| **Data Processing Requirements** | Typically produces denser data, requiring more time and computational resources to process. | Generates lighter datasets but may require additional corrections for motion artefacts. |
| **Suitability for Tight Timelines** | Less suitable for time-sensitive projects due to slower data acquisition. | Well-suited for time-critical tasks requiring rapid scanning and immediate results. |
| **Error Risks** | Lower risk of errors due to stability, but blind spots may occur in inaccessible regions. | Higher risk of errors from trajectory planning and motion-related inconsistencies. |
| **Cost Efficiency** | Higher costs due to slower operations and the potential need for multiple setups in large areas. | More cost-efficient for large-scale or time-sensitive operations. |

Static LiDAR excels in producing high-density point clouds with high precision because of its stationary nature and good precision.

## 4.6 Discussion

### 4.6.1 Identifying and Mapping Rock Deformation in the Underground Mining Environment

The colour-coded visualisation of the deformation patterns presented in Figures 24 -26, effectively highlighted the areas of material loss and bulging, aligning well with field observations. However, the discrepancies noted between the static and mobile LiDAR outputs call for deeper root cause analysis.

The static LiDAR achieved superior accuracy for vertical surfaces (e.g., tunnel walls) due to its stable positioning and point density, this corroborates with findings by Kersten & Lindstaedt (2022) on the advantages of fixed terrestrial scanners in controlled environments. On the contrary, its susceptibility to occlusion (Figure 22) aligns with Farella (2016), Who noted that stationary setups struggle with shadow effects in geometrically complex tunnels.

Mobile LiDAR's streaky point distribution (Figure 21) and higher surface errors resulted from motion-induced noise; a limitation highlighted by Singh et al. (2023) for handheld SLAM systems. Despite this, its ability to capture horizontal surfaces, such as the roof, more accurately than the static LiDAR challenges assumptions by Trzeciak & Brilakis (2021) that mobile systems are less reliable for overhead features.

While static LiDAR's precision is ideal for high-risk zones, requiring millimetre-level accuracy such as unstable roof sections, mobile LiDAR's rapid deployment (Table 11) makes it ideal for time-sensitive applications such as post-blast inspections, where minor errors are acceptable (Rahimi *et al.*, 2020)

### 4.6.2 Comparative Analysis of Deformation Measurement Accuracy

The RMSE and MAE values (Tables 6 and 7) showed static LiDAR's marginally better alignment with field measurements, but the statistical significance ($p<0.05$) requires scrutiny. While the differences between the platforms were statistically insignificant, the

static LiDAR's lower MAE (0.01489 vs 0.01587) could be decisive in high-risk mining environments such as monitoring roof stability in coal seams, where cm errors may trigger safety interventions (Molinda & Mark, 2010). The $R^2$ values of this study are greater than 0.99 for both mobile and static systems, they exceed the findings of (Woolmer *et al.*, 2020) in their mobile LiDAR study in an underground environment. This can be attributed to advancements in SLAM algorithms.

### 4.6.3 Operational Efficiency and Trade-offs of Static and Mobile LiDAR Systems

The trade-offs between accuracy and efficiency (Table 8) contextualised within mining workflows suggest that the slow data acquisition of static LiDAR limits its use to critical and localised inspections. This is concurrent with Chen *et al.* (2022) suggestions for precision application. Mobile LiDAR's speed advantage aligns with Zlot and Bosse's (2014) findings in time-critical events, such as post-disaster assessments, but this efficiency is traded off for lesser data quality. For example, a lower point density near tunnel walls could result in missing fine cracks (Figure 21).

### 4.6.4 Assessment of Data Quality Limitations

The study's data experienced data gaps and meshing errors (Figures 20–22), which affected mobile LiDAR due to its low point density, introducing false deformation signals. Mobile LiDAR's motion artefacts and uneven trajectory overlaps increased interpolation errors during the meshing process, a problem echoed by Del Duca and Machado (2023) in surface reconstruction workflows. Regions with sparse data, such as ridges of uneven surfaces, showed false deformations (Figure 24). Lindenbergh & Pietrzyk (2015b) warns about the effects of relying on data with errors in deformation monitoring.

## 4.7 Limitations and Systematic Biases

While the study achieved its set objectives, the presence of critical limitations cannot be ignored.

The low point density in mobile LiDAR presented by streaky uneven point distribution (Figure 21) leads to interpolation errors during the meshing phase, underestimating deformations (Table 5). This bias risks missing early-stage cracks in high-stress zones. The occlusion in static LiDAR due to its fixed position (Figure 22) created blind spots near the tunnel roof, masking deformations in occluded regions.

These limitations highlight the need for hybrid deployments to cross-validate results and mitigate platform-specific biases.

### 4.8 Cost-Efficiency Analysis

As a cost-benefit framework, the suggests the consideration of the set-up costs, where static LiDARs require multiple stations incurring high costs, for time spent setting up and scanning. Mobile LiDAR requires a single operator and less time for scanning, but data quality is compromised for faster acquisition. When considering accuracy-critical regions, the trade-off is lower cost rates. Mobile LiDAR requires a single operator and less time for scanning, but data quality is compromised for faster acquisition. When considering accuracy-critical regions, the trade-off is lower cost rates. For large mines, mobile LiDAR reduces labour costs but risks higher long-term remediation expenses if deformations are missed. Therefore, a hybrid approach balances upfront costs and risk mitigation.

# Chapter 5

# 5 Conclusion and Recommendations

## 5.1 Introduction

This experimental study aimed to compare the efficiency of mobile and static LiDAR in detecting rock deformation in underground mines. In our analysis, static LiDAR achieved a higher accuracy with an RMSE of 0.0180 vs. 0.0186 for mobile LiDAR. Mobile LiDAR excelled in operational efficiency. The experimental research answered the hypothesis and the null hypothesis. To which the findings accepted the Null hypothesis (p=0.188).

Null Hypothesis ($H_0$):

There is no significant difference between mobile and static LiDAR systems in terms of accuracy for detecting and mapping rock deformation in underground mining environments.

The acceptance indicates no statistical difference in accuracy between the two platforms. However, the practical implications of minor accuracy disparities in safety-critical mining contexts require careful consideration.

## 5.2 Actionable Recommendations

To translate findings into actionable practice, the following actions are proposed:

- To improve data quality, trajectory optimisation can be achieved by the application of real-time gap detection algorithms during mobile scanning to reduce voids (Chen et al., 2022).
- Combining weekly static scanning for accuracy with daily mobile LiDAR scanning for coverage.
- The development of operator certificates, focusing on underground challenges such as occlusion management, trajectory planning, etc., aimed at reducing set-up and scanning errors.
- The integration of the latest algorithms that reduce interpolation errors.

## 5.3 Conclusion

This research successfully addressed its objectives by demonstrating that both static and mobile LiDAR can effectively identify and map underground deformation, provide reliable accuracy in comparison to field measurements, and offer distinct operational efficiencies. A paired t-test at a 5% significance level ($\alpha = 0.05$) was performed to compare the two systems, with the null hypothesis ($H_0$) stating that there is no difference in accuracy between static and mobile LiDAR under the tested conditions, and the alternative hypothesis ($H_1$) stating that a difference exists. The test produced a t-statistic corresponding to a p-value of 0.188, which is greater than the 0.05 significance threshold. Therefore, we fail to reject $H_0$ and conclude that there is no statistically significant difference between the accuracy of the two platforms.

Nonetheless, in scenarios demanding high precision—such as monitoring shafts and roof strata—static LiDAR's superior point density and accuracy make it the preferred option. In contrast, mobile LiDAR's rapid acquisition speed and adaptability make it more suitable for low-risk or extensive coverage zones. The findings underscore the need for deployment strategies that balance safety, cost, and precision. This framework supports enhanced mine safety management and operational sustainability, while offering practical guidance for selecting the appropriate LiDAR system based on the unique requirements of underground mining projects. Future work should explore multi-temporal scanning, improved trajectory optimisation, and advanced processing techniques to further refine LiDAR-based deformation monitoring approaches.

# 6 References


Agapito, J.F.T. & Gilbride, L.J., 2002. Horizontal Stresses as Indicators of Roof Stability. In *2002 SME Annual Meeting*. Society for Mining, Metallurgy, and Exploration. SME, Pheonix, Arizona, pp.01–11. Available at: https://www.agapito.com/wp-content/uploads/2010/05/Horizontal-Stresses-as-Indicators-of-Roof-Stability.pdf [Accessed March 7, 2024].

Ajayi, O. & Palmer, M., 2020. Modelling 3D Topography by Comparing Airborne Lidar Data with Unmanned Aerial System (UAS) Photogrammetry Under Multiple Imaging Conditions. *Geoplanning Journal of Geomatics and Planning*, 6, pp. 122–138.

Alzahrani, A.A.M., 2017. *Detection of mine roof failure using inexpensive LiDAR technology*. Master Of Science. Missouri University of Science and Technology, Missouri. Available at: https://www.proquest.com/openview/4fd1d71565020fcada40e54fa72783bf/1?pq-origsite=gscholar&cbl=18750 [Accessed July 12, 2024].

Artan, U., Marshall, J.A. & Lavigne, N.J., 2011. Robotic mapping of underground mine passageways. *Mining Technology*, 120(1), pp. 18–24.

Atif, I., Cawood, F.T. & Mahboob, M.A., 2021. Development of Interactive Dashboards and Intelligent Data Analytics for Visual Decision-Making in The Underground Mining Environment: The Sterkfontein Cave Case Study. In *2021 International Bhurban Conference on Applied Sciences and Technologies (IBCAST)*. 2021 International Bhurban Conference on Applied Sciences and Technologies (IBCAST). pp.383–388. Available at: https://ieeexplore.ieee.org/abstract/document/9393017 [Accessed July 10, 2024].

Babanouri, N., Beyromvand, H. & Dehghani, H., 2023. Evaluation of different methods of pillar recovery in coal mining by numerical simulation: a case study. *Environmental Earth Sciences*, 82(4), p. 110.

Baggett, J., Abbasi, A., Monsalve, J., Bishop, R., Ripepi, N. & Hole, J., 2020. Ground-Penetrating Radar for Karst Detection in Underground Stone Mines. *Mining, Metallurgy & Exploration*, 37(1), pp. 153–165.

Baghbadorani, A.A., Hole, J.A., Baggett, J. & Ripepi, N., 2021. Radar imaging of fractures and voids behind the walls of an underground mine. *Geophysics*. Available at: https://library.seg.org/doi/10.1190/geo2020-0763.1 [Accessed June 3, 2024].

Bazaluk, O., Rysbekov, K., Nurpeisova, M., Lozynskyi, V., Kyrgizbayeva, G. & Turumbetov, T., 2022. Integrated Monitoring for the Rock Mass State During Large-Scale Subsoil Development. *Frontiers in Environmental Science*, 10. Available at: https://www.frontiersin.org/articles/10.3389/fenvs.2022.852591 [Accessed June 11, 2024].

Benton, D.J., Iverson, S.R., Martin, L.A., Johnson, J.C. & Raffaldi, M.J., 2016. Volumetric measurement of rock movement using photogrammetry. *International Journal of Mining Science and Technology*, 26(1), pp. 123–130.

Bishop, R., Monsalve, J.J., Baggett, J., Soni, A. & Ripepi, N., 2019. A Comparison of Laser Scanning and Photogrammetry in an Underground Limestone Mine. In In 2019 SME Annual Conference and Expo and CMA 121st National Western Mining Conference. Denver, Colorado, pp.19–095.

Bosse, M. & Zlot, R., 2009. Continuous 3D scan-matching with a spinning 2D laser. In *2009 IEEE International Conference on Robotics and Automation*. IEEE, pp.4312–4319.

Braunová, H., Braun, J., Váchová, H. & Kuric, I., 2023. Complex determination of automatic robotic total stations' measurements' accuracy in underground spaces and comparison with results on the surface. | Acta Montanistica Slovaca | EBSCOhost. , 28(3), p. 752. Available at: https://openurl.ebsco.com/contentitem/doi:10.46544%2FAMS.v28i3.18?sid=ebsco:plink:crawler&id=ebsco:doi:10.46544%2FAMS.v28i3.18 [Accessed July 8, 2024].

Brink, V.F., Fourie, F., Mine, K. & Zaniewski, T., 2008. Continuous Monitoring for Safety, Health and Optimisation in South African Deep Level Mining. *Southern African Institute of Mining and Metallurgy*, pp. 1–15.

Broere, W., 2024. Smart monitoring of tunnels. In pp.19–29.

Cai, M., 2024. Rockburst risk control and mitigation in deep mining. *Deep Resources Engineering*, 1(2), p. 100019.

Carter, J., Schmid, K., Waters, K., Betzhold, L., Hadley, B., Mataosky, R. & Halleran, J., 2012. An introduction to LiDAR technology, data, and applications. *NOAA Coastal Services Center*, 2.

Cascante, I., Pérez Martínez, J.J. & Laka, M., 2020. Advanced Techniques for Fast and Accurate Heritage Digitisation in Multiple Case Studies. *Sustainability*, 12, p. 6068.

CDC, 2024. Mining and Ground Falls. *Mining*. Available at: https://www.cdc.gov/niosh/mining/topics/ground-falls.html [Accessed February 25, 2025].

Chaulya, S.K. & Prasad, G.M., 2016. Chapter 7 - Application of Cloud Computing Technology in Mining Industry. In S. K. Chaulya & G. M. Prasad, eds. *Sensing and Monitoring Technologies for Mines and Hazardous Areas*. Elsevier, pp.351–396. Available at: https://www.sciencedirect.com/science/article/pii/B9780128031940000076 [Accessed June 19, 2024].

Chen, B., 2020. Stress-induced trend: the clustering feature of coal mine disasters and earthquakes in China. *International Journal of Coal Science & Technology*, 7(4), pp. 676–692.

Chen, J., Wang, Z., Wu, X., Chen, X., Lai, C., Zeng, Z. & Li, J., 2019. Accuracy evaluation of GPM multi-satellite precipitation products in the hydrological application over alpine and gorge regions with sparse rain gauge network. *Hydrology Research*, 50.

Chen, Y., Zhang, Z., Cao, C., Bao, S., Wang, S. & Xu, G., 2023. Research on the causal mechanism of a rock burst accident in a longwall roadway and its prevention measures. *Scientific Reports*, 13(1), p. 22312.

Chen, Z., Xu, A., Sui, X., Wang, C., Wang, S., Gao, J. & Shi, Z., 2022. Improved-UWB/LiDAR-SLAM Tightly Coupled Positioning System with NLOS Identification Using a LiDAR Point Cloud in GNSS-Denied Environments. *Remote Sensing*, 14(6), p. 1380.

Cota, R.F. & de Figueiredo, R.P., 2014. Borehole Camera And Extensometers To Study Hanging Wall Stability–Case Study Using Voussoir beam-Cuiabá Mine. In *ISRM Brazilian Symposium on Rock Mechanics-SBMR*. ISRM, p.ISRM-SBMR-2014-006.

Council National Research, Virginia, C. on U.M. in & Resources, C. on E., 2011. Potential Environmental Effects of Uranium Mining, Processing, and Reclamation. In *Uranium Mining in Virginia: Scientific, Technical, Environmental, Human Health and Safety, and Regulatory Aspects of Uranium Mining and Processing in Virginia*. National Academies Press (US). Available at: https://www.ncbi.nlm.nih.gov/books/NBK201052/ [Accessed June 21, 2024].

Cowling, N., 2023. South Africa: value added to GDP by mining 2016-2022. Available at: https://www.statista.com/statistics/1121214/mining-sectors-value-added-to-gdp-in-south-africa/ [Accessed December 1, 2023].

Dan, M., Mohamad, E. & Komoo, I., 2016. Characteristics of boulders formed in tropical weathered granite: A review. *Jurnal Teknologi*, 78, pp. 23–30.

Dan, M.F.M., Mohamad, E.T. & Komoo, I., 2016. Characteristics of boulders formed in tropical weathered granite: A review. *Jurnal Teknologi*, 78(8–6).

de Santis, F., Renaud, V., Contrucci, I., Gunzburger, Y. & Bernard, P., 2019. Rock mass behavior in deep mines: in situ monitoring and numerical modelling. In *ISRM Congress*. 14. International congress of rock mechanics. ISMR, Foz do Iguassu, Brazil. Available at: https://ineris.hal.science/ineris-03237766.

Del Duca, G. & Machado, C., 2023. Assessing the Quality of the Leica BLK2GO Mobile Laser Scanner versus the Focus 3D S120 Static Terrestrial Laser Scanner for a Preliminary Study of Garden Digital Surveying. *Heritage*, 6(2), pp. 1007–1027.

Delaloye, D., 2012. *Development of a New Methodology for Measuring Deformation in Tunnels and Shafts With Terrestrial Laser Scanning (LiDAR) Using Elliptical Fitting*

*Algorithms*. thesis. Queen's University, Kingston, Ontario, Canada. Available at: https://qspace.library.queensu.ca/handle/1974/7202 [Accessed April 13, 2021].

Deng, J., Kanwar, N.S., Pandey, M.D. & Xie, W.-C., 2019. Dynamic buckling mechanism of pillar rockbursts induced by stress waves. *Journal of Rock Mechanics and Geotechnical Engineering*, 11(5), pp. 944–953.

Dewez, T.J., Yart, S., Thuon, Y., Pannet, P. & Plat, E., 2017. Towards cavity-collapse hazard maps with Zeb-Revo handheld laser scanner point clouds. *The Photogrammetric Record*, 32(160), pp. 354–376.

DMRE, 2021. *Accident Reports*, Department of Mineral Resources and Energy. Available at: https://www.dmr.gov.za/resources.

Duarte, J., Rodrigues, F. & Castelo Branco, J., 2022. Sensing technology applications in the mining industry—a systematic review. *International Journal of Environmental Research and Public Health*, 19(4), p. 2334.

East, A., 2025. Deadly start to 2025: Global mining fatalities surge. *Mining.com.au*. Available at: https://mining.com.au/deadly-start-to-2025-global-mining-fatalities-surge/ [Accessed February 25, 2025].

Farella, Elisa Mariarosaria, 2016. 3D mapping of underground environments with a hand-held laser scanner. *Bollettino della società italiana di fotogrammetria e topografia*, (2), pp. 1–10.

Farella, E. M., 2016. 3D Mapping of underground environments with a hand-held laser scanner. In *Proceedings of the SIFET Annual Conference*.

Fekete, S., Diederichs, M. & Lato, M., 2009. Geotechnical applications of Lidar scanning in tunnelling. *RockEng. Diederichs and Grasselli, Toronto*, pp. 1–12.

Fröhlich, C. & Mettenleiter, M., 2004. Terrestrial laser scanning-new perspectives in 3D surveying. *International Archives of Photogrammetry, Remote Sensing and Spatial Information Sciences*, 36.

Fryskowska-Skibniewska, A. & Wróblewski, P., 2018. Mobile Laser Scanning accuracy assessment for the purpose of base-map updating. *Geodesy and Cartography*, 67, pp. 35–55.

Fuad, N.A., Ismail, Z., Majid, Z., Darwin, N., Ariff, M.F.M., Idris, K.M. & Yusoff, A.R., 2018. Accuracy evaluation of digital terrain model based on different flying altitudes and conditional of terrain using UAV LiDAR technology. *IOP Conference Series: Earth and Environmental Science*, 169(1), p. 012100.

Garré, S., Blanchy, G., Caterina, D., De Smedt, P., Romero-Ruiz, A. & Simon, N., 2023. Geophysical methods for soil applications. In M. J. Goss & M. Oliver, eds. *Encyclopedia of Soils in the Environment (Second Edition)*. Academic Press, Oxford, pp.444–458. Available at:

https://www.sciencedirect.com/science/article/pii/B978012822974300152X [Accessed June 25, 2024].

Ghorbani, M., Shahriar, K., Sharifzadeh, M. & Masoudi, R., 2020. A critical review on the developments of rock support systems in high stress ground conditions. *International Journal of Mining Science and Technology*, 30(5), pp. 555–572.

Gikas, V., 2012a. Three-Dimensional Laser Scanning for Geometry Documentation and Construction Management of Highway Tunnels during Excavation. *Sensors*, 12(8), pp. 11249–11270.

Gikas, V., 2012b. Three-Dimensional Laser Scanning for Geometry Documentation and Construction Management of Highway Tunnels during Excavation. *Sensors (Basel, Switzerland)*, 12(8), pp. 11249–11270.

Girardeau-Montaut, D. (2015). *CloudCompare (version 2.6.1) [GPL software]. EDF R&D, Telecom ParisTech*.

Gokhan, K. & Korkut, Y., 2013. Hardware Design of Seismic Sensors in Wireless Sensor Network. *International Journal of Distributed Sensor Networks*, 9(9), p. 640692.

Gong, H., Kizil, M.S., Chen, Z., Amanzadeh, M., Yang, B. & Aminossadati, S.M., 2019. Advances in fibre optic based geotechnical monitoring systems for underground excavations. *International Journal of Mining Science and Technology*, 29(2), pp. 229–238.

Grahl, C., 2023. Laser Scanner Comparison: Leica RTC360 vs. Next-Generation BLK360. *BIM Learning Center*. Available at: https://bimlearningcenter.com/laser-scanner-comparison-leica-rtc360-vs-next-generation-blk360/ [Accessed March 25, 2025].

Green, G.E. & Mikkelsen, P.E., 1988. Deformation measurements with inclinometers. *Transportation Research Record*, (1169).

Hadjigeorgiou, J. & Potvin, Y., 2023. Ground support guidelines for squeezing ground conditions. *Journal of the Southern African Institute of Mining and Metallurgy*, 123(7), pp. 371–380.

Hao, Y., Wu, Y., P.g., R., Zhang, K., Zhang, H., Chen, Y., Li, M. & Li, P., 2020. New insights on ground control in intelligent mining with Internet of Things. *Computer Communications*, 150, pp. 788–798.

He, M., Wang, Q. & Wu, Q., 2021. Innovation and future of mining rock mechanics. *Journal of Rock Mechanics and Geotechnical Engineering*, 13(1), pp. 1–21.

Hebblewhite, B.K., 2019. Geotechnical risk in mining methods and practice: critical issues and pitfalls of risk management. In *Proceedings of the first international conference on mining geomechanical risk*. Australian Centre for Geomechanics, pp.299–308.

Huang, S., Chen, M., Lu, S., Chen, S. & Zha, Y., 2021. A novel algorithm: fitting a spatial arc to noisy point clouds with high accuracy and reproducibility. *Measurement Science and Technology*, 32(8), p. 085004.

Hull, G., 2017. *Real-time occupancy grid mapping using LSD-SLAM*. Stellenbosch: Stellenbosch University.

Idrobo-Pizo, G.A., Motta, J.M.S. & Sampaio, R.C., 2019. A calibration method for a laser triangulation scanner mounted on a robot arm for surface mapping. *Sensors*, 19(8), p. 1783.

Iskander, M., 2018. Chapter 3 - Geotechnical Underground Sensing and Monitoring. In S. Pamukcu & L. Cheng, eds. *Underground Sensing*. Academic Press, pp.141–202. Available at: https://www.sciencedirect.com/science/article/pii/B9780128031391000035 [Accessed July 28, 2024].

Jacobs, J., 2016. *Creating a technology map to facilitate the process of modernisation throughout the mining cycle*. University of Pretoria, Pretoria. Available at: https://repository.up.ac.za/bitstream/handle/2263/61296/Jacobs_Creating_2017.pdf?sequence=1 [Accessed March 2, 2024].

Jafari, B., Khaloo, A. & Lattanzi, D., 2017. Deformation tracking in 3D point clouds via statistical sampling of direct cloud-to-cloud distances. *Journal of Nondestructive Evaluation*, 36(4), pp. 1–10.

Jennifer, P.D. & Porchelvan, P., 2021. An approach to assessment of post mining-induced seismic hazard in Kolar Gold Fields mines – a review. *Journal of Mines, Metals and Fuels*, 69(3).

Jia, D., Zhang, W. & Liu, Y., 2021. Systematic Approach for Tunnel Deformation Monitoring with Terrestrial Laser Scanning. *Remote Sensing*, 13(17), p. 3519.

Jia, S., Zhan, Z. & Xu, M., 2021. Shearlet-Based Structure-Aware Filtering for Hyperspectral and LiDAR Data Classification. *Journal of Remote Sensing*, 2021. Available at: https://spj.science.org/doi/full/10.34133/2021/9825415 [Accessed July 12, 2024].

Jiang, X., Min, X., Ye, T., Li, X. & Hu, X., 2023. Monitoring the subsidence at different periods in high underground water level coal mine areas using differential interferometric synthetic aperture radar (D-InSAR). *Geocarto International*, 38(1), p. 2215730.

Jianjun, Z., Xun, W., Yanbing, S., Jiangbo, W. & Lee, M.L., 2021. Deformation behavior of mining beneath flat and sloping terrains in mountainous areas. *Geofluids*, 2021, pp. 1–16.

Jing-xiang, G. & Hong, H., 2009. Advanced GNSS technology of mining deformation monitoring. *Procedia Earth and Planetary Science*, 1(1), pp. 1081–1088.

Jones, E., 2020. Mobile LiDAR for underground geomechanics: Learnings from the teens and directions for the twenties. In *Proceedings of the Second International Conference on Underground Mining Technology; Wesseloo, J., Ed*. pp.3–26. Available at: https://scholar.archive.org/work/je3nzcjvtrd5jiy5ifrjml7n34/access/wayback/https://papers.acg.uwa.edu.au/d/2035_0.01_Jones/0.01_Jones.pdf [Accessed July 12, 2024].

Jones, Evan, 2020. Mobile LiDAR for underground geomechanics: learnings from the teens and directions for the twenties. In *Proceedings of the Second International Conference on Underground Mining Technology*. Australian Centre for Geomechanics, Perth, pp.3–26. Available at: https://papers.acg.uwa.edu.au/p/2035_0.01_Jones/ [Accessed May 11, 2021].

Jones, E., Ghabraie, B. & Beck, D., 2018. A Method for Determining Field Accuracy of Mobile Scanning Devices for Geomechanics Applications. In *ISRM International Symposium-10th Asian Rock Mechanics Symposium*. International Society for Rock Mechanics and Rock Engineering.

Judeel, G.D.T., 2003. Study of the effects of shaft pillar extraction on a vertical shaft located in highly stratified and poor quality rock masses. In *ISRM*. 10th International Congress on Rock Mechanics. Johannesburg, South Africa, pp.587–594. Available at: https://www.researchgate.net/publication/281207544_Study_of_the_effects_of_shaft_pillar_extraction_on_a_vertical_shaft_located_in_highly_stratified_and_poor_quality_rock_masses [Accessed August 15, 2024].

Kang, Z., Zhang, L., Tuo, L., Wang, B. & Chen, J., 2014. Continuous Extraction of Subway Tunnel Cross Sections Based on Terrestrial Point Clouds. *Remote Sensing*, 6(1), pp. 857–879.

Kavvadas, M.J., 2003. Monitoring and modelling ground deformations during tunnelling. In *Proceedings of the 11th FIG Symposium on Deformation Measurements*. pp.371–390.

Keitaanniemi, A., Virtanen, J.-P., Rönnholm, P., Kukko, A., Rantanen, T. & Vaaja, M.T., 2021. The Combined Use of SLAM Laser Scanning and TLS for the 3D Indoor Mapping. *Buildings*, 11(9), p. 386.

Kentucky Geological Survey, 2019. *Kentucky Geological Survey 2018-2019 annual report*, Kentucky Geological Survey, Kentucky, USA. Available at: https://kgs.uky.edu/kygeode/services/pubs/moreinfo.asp?titleInput=18004&map=0.

Kersten, T. & Lindstaedt, M., 2022. Geometric accuracy investigations of terrestrial laser scanner systems in the laboratory and in the field. *Applied Geomatics*, 14, pp. 421–434.

Khan, M., Xueqiu, H., Farid, A., Jianqiang, C., Honglei, W., Dazhao, S. & Chao, Z., 2022. Geophysical Characterization of Mining-Induced Complex Geological Deformations in a Deep Coalmine. *Lithosphere*, 2021(Special 4), p. 7564984.

Kim, E.M. & Seo, H.D., 2020. Registration of Three-Dimensional Point Clouds Based on Quaternions Using Linear Features. *Journal of the Korean Society of Surveying, Geodesy, Photogrammetry and Cartography*, 38(3), pp. 175–185.

Kolapo, P., 2020. *Towards a short-range laboratory for testing the accuracy of terrestrial 3D laser scanning (TLS) technologies*.

Kouzehgar, K. & Eslamian, S., 2023. Chapter 2 - Application of experimental data and soft computing techniques in determining the outflow and breach characteristics in embankments and landslide dams. In S. Eslamian & F. Eslamian, eds. *Handbook of Hydroinformatics*. Elsevier, pp.11–31. Available at: https://www.sciencedirect.com/science/article/pii/B9780128219621000027 [Accessed February 23, 2025].

Kuester, M., Intaratep, N. & Borgoltz, A., 2018. Laser Displacement Sensors for Wind Tunnel Model Position Measurements. *Sensors (Basel, Switzerland)*, 18(12), p. E4085.

Kumar, D., 2010. Emerging Tools and Techniques for Mine Safety and Disaster Management. In M. K. Jha, ed. *Natural and Anthropogenic Disasters: Vulnerability, Preparedness and Mitigation*. Springer Netherlands, Dordrecht, pp.332–365. Available at: https://doi.org/10.1007/978-90-481-2498-5_15 [Accessed June 20, 2024].

Lague, D., Brodu, N. & Leroux, J., 2013. Accurate 3D comparison of complex topography with terrestrial laser scanner: Application to the Rangitikei canyon (N-Z). *ISPRS Journal of Photogrammetry and Remote Sensing*, 82, pp. 10–26.

Leica Geosystems, 2019. What is a total station and how it works? Available at: https://cpe.leica-geosystems.com/us/blog/post/what-is-a-total-station-how-it-works.html [Accessed June 25, 2024].

Li, X., Du, S., Li, G. & Li, H., 2020. Integrate Point-Cloud Segmentation with 3D LiDAR Scan-Matching for Mobile Robot Localization and Mapping. *Sensors*, 20(1), p. 237.

Li, X., Wang, Y., Hu, Y., Zhou, C. & Zhang, H., 2022. Numerical Investigation on Stratum and Surface Deformation in Underground Phosphorite Mining Under Different Mining Methods. *Frontiers in Earth Science*, 10. Available at: https://www.frontiersin.org/articles/10.3389/feart.2022.831856 [Accessed June 6, 2024].

Lin, C., Liu, H., Wu, D. & Gong, B., 2020. Background point filtering of low-channel infrastructure-based LiDAR data using a slice-based projection filtering algorithm. *Sensors*, 20(11), p. 3054.

Lindenbergh, R. & Pietrzyk, P., 2015a. Change detection and deformation analysis using static and mobile laser scanning. *Applied Geomatics*, 7(2), pp. 65–74.

Lindenbergh, R. & Pietrzyk, P., 2015b. Change detection and deformation analysis using static and mobile laser scanning. *Applied Geomatics*, 7(2), pp. 65–74.

Malberg, K., 2019. *Determining the Shape and Volume of Enclosed Spaces and Underground Mines by Mobile Laser Scanning*. MSc Thesis. Tallinn University of Technology, Tallinn. Available at: https://digi.lib.ttu.ee/i/?12484 [Accessed April 21, 2021].

Małkowski, P., Niedbalski, Z., Majcherczyk, T. & Bednarek, Ł., 2020. Underground monitoring as the best way of roadways support design validation in a long time. *Mining of Mineral Deposits*, 14(3), pp. 1–14.

Mariusz, W. & Zbigniew, R., 2014. *Comparison of laser distance measuring instruments*, EURAMET. Available at: https://www.bipm.org/documents/20126/45452739/EURAMET.L-S20.pdf/33fcd3cb-634e-e1b8-c1ae-b3d2e050d7a0 [Accessed January 10, 2022].

Mark, C., 2016. Coal bursts in the deep longwall mines of the United States. *International Journal of Coal Science & Technology*, 3(1), pp. 1–9.

MHSC, 2023. *The pursuit of zero harm continues*, Mining Health and Safety Council. Available at: https://mhsc.org.za/legislation/ [Accessed December 1, 2023].

Mohindru, G., Mondal, K. & Banka, H., 2020. Internet of Things and data analytics: A current review. *WIREs Data Mining and Knowledge Discovery*, 10(3), p. e1341.

Molinda, G. & Mark, C., 2010. Ground Failures in Coal Mines with Weak Roof. *Electron J Geotech Eng*, 15(F), pp. 547–588.

Monika, Govil, H. & Guha, S., 2023. Underground mine deformation monitoring using Synthetic Aperture Radar technique: A case study of Rajgamar coal mine of Korba Chhattisgarh, India. *Journal of Applied Geophysics*, 209, p. 104899.

Morales, J., Plaza-Leiva, V., Mandow, A., Gomez-Ruiz, J.A., Serón, J. & García-Cerezo, A., 2018. Analysis of 3D Scan Measurement Distribution with Application to a Multi-Beam Lidar on a Rotating Platform. *Sensors (Basel, Switzerland)*, 18(2), p. 395.

Newman, C., Agioutantis, Z. & Boede Jimenez Leon, G., 2017. Assessment of potential impacts to surface and subsurface water bodies due to longwall mining. *International Journal of Mining Science and Technology*, 27(1), pp. 57–64.

Ng, A.H.-M., Ge, L., Zhang, K., Chang, H.-C., Li, X., Rizos, C. & Omura, M., 2011. Deformation mapping in three dimensions for underground mining using InSAR – Southern highland coalfield in New South Wales, Australia. *International Journal of Remote Sensing*, 32(22), pp. 7227–7256.

NSW Government Agency, 2021. Geotechnical Instrumentation and Monitoring Guidelines. Available at: https://www.transport.nsw.gov.au/system/files?file=media/asa_standards/2021/t-mu-ci-12140-gu-v2.0.pdf.

NSWG, 2023. *Rockfall injuries to workers increase in underground mines*, Resources Regulator Department of Regional NSW, North South Wales. Available at: https://www.resourcesregulator.nsw.gov.au/sites/default/files/2023-06/sb23-06-rockfall-injuries-to-workers-increase-in-underground-mines.pdf [Accessed July 28, 2024].

Onifade, M., Zvarivadza, T. & Adebisi, J.A., 2024. Towards application of positioning systems in the mining industry. *International Journal of Mining and Mineral Engineering*, 15(1), pp. 15–48.

Onyutha, C., 2020. *From R-squared to coefficient of model accuracy for assessing 'goodness-of-fits'*,

Padmanabhan, P., Zhang, C. & Charbon, E., 2019. Modeling and analysis of a direct time-of-flight sensor architecture for LiDAR applications. *Sensors*, 19(24), p. 5464.

Pawlik, M., Haske, B., Flores, H., Bernsdorf, B. & Rudolph, T., 2024. Towards a Long-Term Unmanned Aerial Vehicle (UAV) Monitoring Framework for Post-Mining Effects: Prosper-Haniel Case. *Mining*, 4(2), pp. 211–229.

Pawluszek-Filipiak, K. & Borkowski, A., 2021. Monitoring mining-induced subsidence by integrating differential radar interferometry and persistent scatterer techniques. *European Journal of Remote Sensing*, 54(sup1), pp. 18–30.

Pinpin, L., Wenge, Q., Yunjian, C. & Feng, L., 2021. Application of 3D Laser Scanning in Underground Station Cavity Clusters. *Advances in Civil Engineering*, 2021(1), p. 8896363.

Procházková, J. & Martišek, D., 2018. Notes on Iterative Closest Point Algorithm.

Pu, Y., Apel, D.B., Liu, V. & Mitri, H., 2019. Machine learning methods for rockburst prediction-state-of-the-art review. *International Journal of Mining Science and Technology*, 29(4), pp. 565–570.

Quadros, N., Collier, P. & Fraser, C., 2008. Integration of Bathymetric and Topographic LIDAR: A Preliminary Investigation. *Remote Sensing and Spatial Information Sciences*, 37.

Rahimi, B., Sharifzadeh, M. & Feng, X.-T., 2020. Ground behaviour analysis, support system design and construction strategies in deep hard rock mining – Justified in Western Australian's mines. *Journal of Rock Mechanics and Geotechnical Engineering*, 12(1), pp. 1–20.

Rashdi, R., Garrido, I., Balado, J., Del Río-Barral, P., Rodríguez-Somoza, J.L. & Martínez-Sánchez, J., 2024. Comparative Evaluation of LiDAR systems for transport infrastructure: case studies and performance analysis. *European Journal of Remote Sensing*, 57(1), p. 2316304.

Ratsheko, T.T., 2018. *A critical analysis of the extent to which SA law protects the surface rights of landowners over whose property mining rights have been granted*. University of Pretoria, Pretoria. Available at: https://repository.up.ac.za/bitstream/handle/2263/69981/Ratsheko_Critical_2018.pdf?sequence=1&isAllowed=y [Accessed June 21, 2024].

Riemer, K.L. & Durrheim, R.J., 2012. Mining seismicity in the Witwatersrand Basin: monitoring, mechanisms and mitigation strategies in perspective. *Journal of Rock Mechanics and Geotechnical Engineering*, 4(3), pp. 228–249.

Ritter, T., Gollob, C. & Nothdurft, A., 2020. Towards an Optimization of Sample Plot Size and Scanner Position Layout for Terrestrial Laser Scanning in Multi-Scan Mode. *Forests*, 11(10), p. 1099.

Romero, A., Gatta, C. & Camps-Valls, G., 2016. Unsupervised Deep Feature Extraction for Remote Sensing Image Classification. *IEEE Transactions on Geoscience and Remote Sensing*, 54(3), pp. 1349–1362.

Russell, T.M. & Stacey, T.R., 2019. Using laser scanner face mapping to improve geotechnical data confidence at Sishen mine. *Journal of the Southern African Institute of Mining and Metallurgy*, 119(1), pp. 11–20.

Sadeghi, S., Soltanmohammadlou, N. & Nasirzadeh, F., 2022. Applications of wireless sensor networks to improve occupational safety and health in underground mines. *Journal of Safety Research*, 83, pp. 8–25.

Salcher, M., 2015. Robust monitoring for high risk underground excavations. In *FMGM 2015: Proceedings of the Ninth Symposium on Field Measurements in Geomechanics*. Australian Centre for Geomechanics, pp.409–422.

Schuhmacher, S. & Böhm, J., 2005. Georeferencing of terrestrial laserscanner data for applications in architectural modeling.

Schulz, T. & Ingensand, H., 2004. Terrestrial Laser Scanning – Investigations and Applications for High Precision Scanning. , p. 15.

Seymour, J., Martin, L., Raffaldi, M., Warren, S. & Sandbak, L., 2019. Long-Term Stability of a 13.7 × 30.5-m (45 × 100-ft) Undercut Span Beneath Cemented Rockfill at the Turquoise Ridge Mine, Nevada. *Rock Mechanics and Rock Engineering*, 2019.

Silvia, E.P. & Olsen, M.J., 2012. To Level or Not to Level: Laser Scanner Inclination Sensor Stability and Application. *Journal of Surveying Engineering*, 138(3), pp. 117–125.

Singh, S.K., Banerjee, B.P. & Raval, S., 2023. A review of laser scanning for geological and geotechnical applications in underground mining. *International Journal of Mining Science and Technology*, 33(2), pp. 133–154.

Singh, S.K., Banerjee, B.P. & Raval, S., 2021. Three-Dimensional Unique-Identifier-Based Automated Georeferencing and Coregistration of Point Clouds in Underground Mines. *Remote Sensing*, 13(16), p. 3145.

Singh, S.K., Raval, S. & Banerjee, B., 2021. A robust approach to identify roof bolts in 3D point cloud data captured from a mobile laser scanner. *International Journal of Mining Science and Technology*, 31(2), pp. 303–312.

Sirohi, R.S., 2018. *Optical methods of measurement: wholefield techniques*, CRC Press.

Slaker, B., 2015. *Monitoring Underground Mine Displacement Using Photogrammetry and Laser Scanning*. Doctoral Dissertation. Virginia Tech, Virginia. Available at: http://hdl.handle.net/10919/51691 [Accessed July 12, 2024].

Slaker, B.A. & Mohamed, K.M., 2017. A practical application of photogrammetry to performing rib characterization measurements in an underground coal mine using a DSLR camera. *International Journal of Mining Science and Technology*, 27(1), pp. 83–90.

Strzałkowski, P., 2021. Duration of the final phase of mining area deformation process in the conditions of Upper Silesia (Poland). *Bulletin of Engineering Geology and the Environment*, 80(7), pp. 5769–5780.

Suchocki, C., 2020. Comparison of Time-of-Flight and Phase-Shift TLS Intensity Data for the Diagnostics Measurements of Buildings. *Materials*, 13(2), p. 353.

Suh, Y.S., 2019. Laser sensors for displacement, distance and position. *Sensors*, 19(8), p. 1924.

Thomson, C., Apostolopoulos, G., Backes, D. & Boehm, J., 2013. Mobile laser scanning for indoor modelling. *ISPRS Ann. Photogramm. Remote Sens. Spat. Inf. Sci*, 5(W2), p. 66.

Trzeciak, M. & Brilakis, I., 2021. *Comparison of accuracy and density of static and mobile laser scanners*,

Uggla, G. & Horemuz, M., 2021. Towards synthesized training data for semantic segmentation of mobile laser scanning point clouds: Generating level crossings from real and synthetic point cloud samples. *Automation in Construction*, 130, p. 103839.

van der Merwe, J.W. & Andersen, D.C., 2013a. Applications and benefits of 3D laser scanning for the mining industry. *Journal of the Southern African Institute of Mining and Metallurgy*, 113(3), pp. 00–00.

van der Merwe, J.W. & Andersen, D.C., 2013b. Applications and benefits of 3D laser scanning for the mining industry. *Journal of the Southern African Institute of Mining and Metallurgy*, 113(3), pp. 00–00.

Vazaios, I., Farahmand, K., Vlachopoulos, N. & Diederichs, M., 2018. Effects of confinement on rock mass modulus: A synthetic rock mass modelling (SRM) study. *Journal of Rock Mechanics and Geotechnical Engineering*, 10, pp. 436–456.

Wagner, H., 2019. Deep Mining: A Rock Engineering Challenge. *Rock Mechanics and Rock Engineering*, 52(5), pp. 1417–1446.

Wajs, J., Kasza, D., Zagożdżon, P.P. & Zagożdżon, K.D., 2018. 3D modeling of underground objects with the use of SLAM technology on the example of historical mine in Ciechanowice (Ołowiane Range, The Sudetes) T. A. Przylibski & D. Kasza, eds. *E3S Web of Conferences*, 29, p. 00024.

Walker, D., 2023. Benefits of Deformation Monitoring for Modern Infrastructure & using Drones. *Crucial Services*. Available at: https://crucialservices.net/benefits-of-deformation-monitoring-drones-for-modern-infrastructure/ [Accessed February 16, 2024].

Wang, C., Xiao, Z., Wang, Y., Wang, F. & Li, Z., 2024. Big data acquisition for underground infrastructure condition assessment. *Data-Centric Engineering*, 5, p. e49.

Wang, J., Zheng, H.B., Huang, H. & Ma, G.W., 2017. Point Cloud Modelling Based On The Tunnel Axis And Block Estimation For Monitoring The Badaling Tunnel, China. In *The International Archives of the Photogrammetry, Remote Sensing and Spatial Information Sciences*. Wuhan, China, pp.301–306.

Wang, L. & Fang, N., 2017. *Applications of Fiber-Optic Interferometry Technology in Sensor Fields*, IntechOpen. Available at: https://www.intechopen.com/chapters/53137 [Accessed January 12, 2022].

Wang, M., Zhou, J., Shi, A., Han, J. & Li, H., 2020. Key Factors Affecting the Deformation and Failure of Surrounding Rock Masses in Large-Scale Underground Powerhouses. *Advances in Civil Engineering*, 2020, p. e8843466.

Wang, Q., Tan, Y. & Mei, Z., 2020. Computational methods of acquisition and processing of 3D point cloud data for construction applications. *Archives of computational methods in engineering*, 27(2), pp. 479–499.

Wang, T., Chen, C., Xia, K., Shao, Y., Liu, X. & Yang, K., 2023. Ground movement in the hanging wall of underground iron mines with steeply dipping discontinuities: a case study. *Arabian journal for science and engineering*, 48(10), pp. 13465–13488.

Wang, Y., Wang, X., Zhang, J., Chen, X., Zhu, W. & Zhang, Y., 2021. Roof subsidence and movement law of composite strata mining: insights from physical and numerical modeling. *Minerals*, 12(1), p. 3.

Wang, Y., Zhang, Z., Ren, Q., Wu, Y. & Peng, Z., 2012. Application of LTD-2100 ground penetrating radar to advanced forecast in diversion tunnel of Jinping Hydroelectric power Station. In *2012 14th International Conference on Ground Penetrating Radar (GPR)*. 2012 14th International Conference on Ground Penetrating Radar (GPR). pp.57–61. Available at: https://ieeexplore.ieee.org/abstract/document/6254832 [Accessed July 11, 2024].

Webber-Youngman, R., Grobler, H., Gazi, T., Stroh, F. & van der Vyver, A., 2019. The impact of forensic laser scanning technology on incident investigations in the mining industry. *Journal of the Southern African Institute of Mining and Metallurgy*, 119(10), pp. 817–824.

Weidong, P., Fancheng, M., Renguo, G., LuoYonglei & Zhengbo, H., 2012. Relationship between Operation Technology of Ground Penetrating Radar and Precision of Advanced Forecast. In *2012 International Conference on Computer Science and Electronics Engineering*. 2012 International Conference on Computer Science and Electronics Engineering. pp.640–644. Available at: https://ieeexplore.ieee.org/abstract/document/6188255 [Accessed July 11, 2024].

Whyte, H.D., 2006. Simultaneous localisation and mapping (SLAM): Part I the essential algorithms. *Robotics and Automation Magazine*.

Woolmer, D., Jones, E., Taylor, J., Baylis, C., Kewe, D., Castro, R., Báez, F. & Suzuki, K., 2020. Use of Drone based Lidar technology at Olympic Dam Mine and initial Technical Applications, University of Chile. Available at: https://papers.acg.uwa.edu.au/p/2063_38_Woolmer/ [Accessed July 12, 2024].

Wu, W., 2021. A review of unloading-induced fault instability. *Underground Space*, 6(5), pp. 528–538.

Xia, K., Chen, C., Liu, X., Fu, H., Pan, Y. & Deng, Y., 2016. Mining-induced ground movement in tectonic stress metal mines: a case study. *Bulletin of Engineering Geology and the Environment*, 75(3), pp. 1089–1115.

Xia, Y., Liu, B., Zhang, C., Liu, N., Zhou, H., Chen, J., Tang, C., Gao, Y., Zhao, D. & Meng, Q., 2022. Investigations of mechanical and failure properties of 3D printed columnar jointed rock mass under true triaxial compression with one free face. *Geomechanics and Geophysics for Geo-Energy and Geo-Resources*, 8, pp. 1–24.

Xu, S., Zhang, P., Zhang, D., Wu, R. & Guo, L., 2015. Simulation study of fiber optic monitoring technology of surrounding rock deformation under deep mining conditions. *Journal of Civil Structural Health Monitoring*, 5(5), pp. 563–571.

Xu, X., Yang, H. & Neumann, I., 2018. Time-efficient filtering method for three-dimensional point clouds data of tunnel structures. *Advances in Mechanical Engineering*, 10(5), p. 1687814018773159.

Yan, B., Guo, Q., Ren, F. & Cai, M., 2020. Modified Nishihara model and experimental verification of deep rock mass under the water-rock interaction. *International Journal of Rock Mechanics and Mining Sciences*, 128, p. 104250.

Yang, Q., Zhang, Z., Liu, X. & Ma, S., 2017a. Development of Laser Scanner for Full Cross-Sectional Deformation Monitoring of Underground Gateroads. *Sensors*, 17(6), p. 1311.

Zare, M., Battulwar, R., Seamons, J. & Sattarvand, J., 2021. Applications of Wireless Indoor Positioning Systems and Technologies in Underground Mining: a Review. *Mining, Metallurgy & Exploration*, 38(6), pp. 2307–2322.

Zeng, W., Huang, Z., Wu, Y., Li, S., Zhang, R. & Zhao, K., 2020. Experimental investigation on mining-induced strain and failure characteristics of rock masses of mine floor. *Geomatics, Natural Hazards and Risk*, 11(1), pp. 491–509.

Zhang, Shizhong, Fan, G., Zhang, D., Li, S., Chen, M., Fan, Y. & Luo, T., 2021. Impacts of longwall mining speeds on permeability of weakly cemented strata and subsurface watertable: a case study. *Geomatics, Natural Hazards and Risk*, 12(1), pp. 3063–3088.

Zhang, Shukun, Lu, L., Wang, Z. & Wang, S., 2021. A physical model study of surrounding rock failure near a fault under the influence of footwall coal mining. *International Journal of Coal Science & Technology*, 8(4), pp. 626–640.

Zhao, J. & Konietzky, H., 2020. Numerical analysis and prediction of ground surface movement induced by coal mining and subsequent groundwater flooding. *International Journal of Coal Geology*, 229, p. 103565.

Zhao, Q., Yang, Z., Jiang, Y., Liu, X., Cui, F. & Li, B., 2023. Discrete element analysis of deformation features of slope controlled by karst fissures under the mining effect: a case study of Pusa landslide, China. *Geomatics, Natural Hazards and Risk*, 14(1), pp. 1–35.

Zhou, W.-H., Guan, Z. & Li, X., 2024. *Geotechnical aspects of underground construction in soft ground*, Taylor & Francis. Available at: https://library.oapen.org/handle/20.500.12657/90828 [Accessed July 11, 2024].

Zhou, Y., Aryal, S. & Bouadjenek, M.R., 2024. A Comprehensive Review of Handling Missing Data: Exploring Special Missing Mechanisms. *arXiv preprint arXiv*, 2404.04905. Available at: https://arxiv.org/html/2404.04905v1.

Zlot, R. & Bosse, M., 2014a. Efficient large-scale 3D mobile mapping and surface reconstruction of an underground mine. In *Field and service robotics*. Springer, pp.479–493.

Zlot, R. & Bosse, M., 2014b. Efficient Large-scale Three-dimensional Mobile Mapping for Underground Mines. *Journal of Field Robotics*, 31(5), pp. 758–779.